Université de Montréal

Study of Langmuir-Blodgett Films of Self-Assembled Diblock Copolymers

par Kateryna Borozenko

Département de chimie
Faculté des arts et des sciences

Mémoire présenté à la Faculté des études supérieures et postdoctorales en vue de l'obtention du grade de maître ès sciences (M.Sc.) en chimie»

Juillet 2015

© Kateryna Borozenko, 2015

Université de Montréal

Faculté des études supérieures et postdoctorales

Ce mémoire intitulé:

Study of Langmuir-Blodgett Films of Self-Assembled Diblock Copolymers

Présenté par:

Kateryna Borozenko

a été évalué par un jury composé des personnes suivantes:

Présidente-rapporteuse: Antonella Badia

Directrice de recherche: Geraldine Bazuin

Codirecteur: Christian Pellerin

Membre du jury: Suzanne Giasson

Résumé

L'auto-assemblage des copolymères à bloc (CPBs) attire beaucoup d'intérêt grâce à leur capacité de générer spontanément des matériaux ordonnés avec des propriétés uniques. Les techniques Langmuir-Blodgett (LB) et Langmuir-Schaefer (LS) sont couramment utilisées pour produire des monocouches ou des films ultraminces à l'interface air/eau suivi de transfert aux substrats solides. Les films LB/LS de CPBs amphiphiles s'auto-assemblent dans des morphologies variables dépendamment de la composition du CPB ainsi que d'autres facteurs. Dans notre travail, nous avons étudié les films LB/LS de polystyrène-*b*-poly(4-vinyl pyridine) (PS-P4VP) et leurs complexes supramoléculaires avec le naphtol (NOH), l'acide naphtoïque (NCOOH) et le 3-*n*-pentadécylphenol (PDP).

La première partie de ce mémoire est consacré à l'investigation du PS-P4VP complexé avec le NOH et le NCOOH, en comparaison avec le PS-P4VP seul. Il a été démontré qu'un plateau dans l'isotherme de Langmuir, indicatif d'une transition de premier ordre, est absent à des concentrations élevées des solutions d'étalement des complexes. Cela a été corrélé avec l'absence de morphologie en nodules avec un ordre 2D hexagonal à basse pression de surface. L'ordre au-delà de la pression de cette transition, lorsque présente, change à un ordre 2D carré pour tout les systèmes.

La deuxième partie du la mémoire considère à nouveau le système PS-P4VP/ PDP, pour lequel on a démontré antérieurement que la transition dans l'isotherme correspond a une transition 2D d'un ordre hexagonal à un ordre carré. Cela est confirmé par microscopie à force atomique, et, ensuite, on a procédé à une étude par ATR-IR des films LB pour mieux comprendre les changements au niveau moléculaire qui accompagnent cette transition. Il a été constaté que, contrairement à une étude antérieure dans la littérature sur un autre système, il n'y a aucun changement dans l'orientation des chaînes alkyles. Au lieu de cela, on a découvert que, aux pressions au-delà de celle de la transition, le groupe pyridine, qui est orienté à basse pression, devient isotrope et qu'il y a une augmentation des liaisons hydrogènes phénol-pyridine. Ces observations sont rationalisées par un collapse partiel à la pression de transition de la monocouche P4VP, qui à basse pression est ordonné au niveau moléculaire.

Cette étude a mené à une meilleure compréhension des mécanismes moléculaires qui se produisent à l'interface air/eau, ce qui fournit une meilleure base pour la poursuite des applications possibles des films LB/LS dans les domaines de nanotechnologie.

Mots-clés : copolymères à bloc, auto-assemblage, Langmuir-Schaefer, Langmuir-Blodgett, isotherme de Langmuir, monocouche, interface air/eau, AFM, ATR-IR, PS-P4VP, PDP, NOH, NCOOH.

Abstract

Self-assembly of block copolymers (BCPs) attracts much interest due to their ability to spontaneously generate ordered materials with unique properties. For many applications, such as masks in nanolithography, separation membranes in medical diagnostics, and nanotemplates for nanowire fabrication, manufacturing into thin films is required. The Langmuir-Blodgett (LB) and Langmuir-Schaefer (LS) techniques are commonly used to produce ultrathin or monolayer films at the air/water interface that are transferred to solid substrates. LB/LS films of amphiphilic BCPs self-assemble into various morphologies, depending on the BCP composition and other factors. In our work, we investigated LB/LS films of polystyrene-*b*-poly(4-vinyl pyridine) (PS-P4VP) and their supramolecular complexes with, naphthol (NOH), naphthoic acid (NCOOH) and 3-*n*-pentadecylphenol (PDP).

The first part of the thesis was devoted to the investigation of PS-P4VP complexes with NOH and NCOOH, in comparison to PS-P4VP alone. It was shown that a plateau in the Langmuir isotherm, indicative of a first-order transition, is absent at high spreading solution concentrations for the complexes. This was correlated with an absence of the expected dot morphology with 2D hexagonal-like order at low surface pressure. Above the transition, when present, the morphology has 2D square order.

The second part of the thesis re-examines the PS-P4VP/PDP system, which was previously shown to undergo a transition from 2D hexagonal to square order at the isotherm plateau pressure. This was confirmed here, and a detailed ATR-IR study of LB films was then undertaken to better understand molecular-level changes occurring at this transition. It was found that, contrary to another study in the literature on a different system, there is no change in alkyl chain orientation. Instead, it was found that the pyridine group loses its low-pressure orientation and there is increased phenol-pyridine hydrogen-bonding above the transition pressure, which is rationalized by a partial collapse of the low-pressure molecularly ordered P4VP monolayer at the transition pressure.

This study leads to an improved understanding of the processes occurring at the air/water interface, which is a basis for the further possible applications of LB/LS films in nanotechnologies.

Keywords : block copolymers, self-assembly, Langmuir-Blodgett, Langmuir-Schaefer, Langmuir isotherm, monolayer, air/water interface, AFM, ATR-IR, PS-P4VP, PDP, NOH, NCOOH.

Table of contents

List of Figures

List of Tables

List of Abbreviations

π	surface pressure
3D	three-dimensional
AFM	atomic force microscopy
ATR-IR	attenuated total reflection infrared spectroscopy
DNA	deoxyribonucleic acid
FFT	fast Fourier transform
HABA	2-(4′-hydroxybenzeneazo)benzoic acid
LB	Langmuir-Blodgett
LS	Langmuir-Schaefer
MSEF	mean square electric field
NCOOH	1-naphthoic acid
NOH	1-naphthol
P4VP	poly(4-vinyl pyridine)
PDP	3-*n*-pentadecylphenol
PS	Polystyrene
PS-P4VP	polystyrene-*b*-poly(4-vinyl pyridine)
PS-PEO	polystyrene-*b*-poly(ethylene oxide)
RNA	ribonucleic acid
SNR	signal-to-noise ratio

Acknowledgements

This thesis work would not be possible without the guidance of my supervisors, Prof. C. Géraldine Bazuin and Prof. Christian Pellerin. I would like to express my gratitude to them for allowing me to carry out this project in their esteemed groups, financial support and coverage of my trips to scientific conferences and for their endless understanding and kindness. I will never forget it.

I acknowledge Marie Richard-Lacroix for her substantial contribution to our collaborative work, her ideas and energy that led our joint project to good results.

I thank Dr. Iryna Perepichka who was the first person who introduced me to the world of polymers, taught me essential skills to work in the laboratory and supported me during my summer internships in 2010 and 2011.

I am grateful to Prof. Antonella Badia and Prof. Géraldine Bazuin for the opportunity, financial support and allowing me to gain valuable experience during my summer internships in 2010 and 2011, which was the starting point of my growing scientific interest to the research.

I am appreciative to all members of both groups, particularly, Anna Gittsegrad, who helped me during my Master's program and thesis editing.

Finally, I express my deep gratitude to my family for their encouragement and constant support, especially, to my sister Olga Borozenko, who defended her Ph.D dissertation in Chemistry in May 2014 at the Université de Montréal, and thereby inspired me to the successful writing of my thesis.

CHAPTER 1

INTRODUCTION

1.1. **Self-assembly of block copolymers**

The tendency to miniaturize of objects has given a powerful impulse to the development of nanoscience and nanotechnology. By itself, nanotechnology is based on the ability to design highly accurate nanostructures and nano-objects with well-defined shape, size and order. There are two general approaches for the creation of such structures: “top-down” and “bottom-up”.[1] The "top-down" approach to nanotechnology involves the creation of "nano-objects" from a parent entity that is larger. This type of fabrication uses traditional workshop or microfabrication methods, such as lithographic patterning techniques, with externally controlled tools. The main problem of such an approach is damage of crystal structure. The “top-down” approach is limited in the smallest dimensions it can reach, especially in a high throughput, cost-effective manner. For small structures, the “bottom-up” approach is very appealing. This approach to nanotechnology uses the molecular self-assembly process based on chemical or physical forces acting at the nanoscale to assemble basic units into larger structures.[2] Self-assembly is the spontaneous association of components into particles or structures without human intervention; it can be static or dynamic. In the case of static self-assembly, the system approaches equilibrium, reducing its free energy. Dynamic self-assembly is the spontaneous and reversible organisation of molecular units into an ordered structure through non-covalent interactions.[3]

The most famous and most visual example of self-assembly occurring in nature is the double-helix of DNA (Figure 1-1a). The single chain of DNA is a sequence of nucleotides consisting of phosphates, sugars and bases. The chains have a helix shape to minimize the contact of water-insoluble parts (bases) with the cell environment. Bases are attached to the sugar-phosphate main chain. To avoid contact with water they tuck themselves into the center of a folded structure. A single chain with this structure leaves large empty spaces between base pairs, which is unacceptable. To solve this, a second helix of DNA provides base pairs to form enthalpically favorable double-stranded chains, where two single chains are held together by hydrogen bonds. Thus adenine (A) forms two hydrogen bonds with

thymine (T) and guanine (G) forms three with cytosine (C) (Figure 1-1b). Thus, due to the additional H-bond, the G-C pair is more stable than the A-T pair.[4,5]

Another example of a well-studied self-assembled natural system is the tobacco mosaic virus (Figure 1-1c)[6]. This rod-shaped virus consists of a series of self-assembled double-layered protein disks with an RNA chain embedded in the central hole of the virus. In order to recognize the protein disks, the RNA chain should have a specific 3D structure and the base pairs must be complementary with the protein sequence of the disk. Only in such conditions will the specific construction of the virus through self-assembly take place.[7-9]

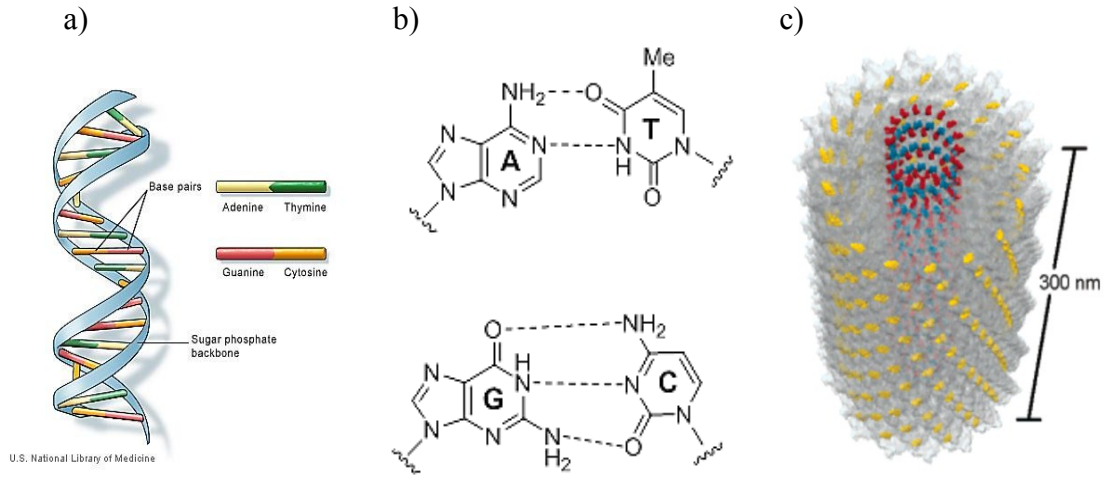

Figure 1-1. Examples of self-assembling structures in nature.

a) Double helix of DNA chains. b) Complementary pairs of DNA nucleotides (dashed lines indicate H-bonding). c) Tobacco mosaic virus. Image *a* is courtesy of the US National Library of Medicine. Image *c* Reprinted with permission from ref. 7. Copyright 2005 American Chemical Society.

In the past century, synthetic polymers have become an essential part of everyday life. Based on the principles of self-assembly borrowed from nature and further applied to polymers, in particular to block copolymers, it became possible to generate highly ordered polymer structures with molecular level control and precision. These self-assembled polymers provide simple, parallel and cost effective processes for nanofabrication.[10,11] The self-assembly of block copolymers

in the bulk and thin films is reviewed in the following sections. Since ultrathin films of block copolymers obtained by the so-called Langmuir-Blodgett (LB) technique is the main subject of the thesis, this technique will then be presented along with molecular orientation determination using an infrared technique (ATR-IR). Previous literature on the morphology of LB monolayers of diblock polymers will then be summarized, to finally present the objectives of this thesis.

1.1.1. Self-assembly in the bulk

Historically, studies of block copolymer self-assembly began with the bulk phase. Bulk block copolymer morphologies are characterized by well-ordered microdomains.[12] Phase separation into microdomains occurs when two blocks are immiscible, and is influenced by the two thermodynamic effects, entropy and enthalpy. Below a critical (order-disorder transition) temperature, an enthalpic effect drives the blocks to phase separate. The entropic effect dominates at temperatures higher than the critical temperature and results in homogenous mixing of the polymer chains.[13] Microscopic phase separation of the blocks promotes the formation of a variety of morphologies, such as spheres (S), cylinders (C), bicontinuous gyroids (G) and lamellae (L) (Figure 1-2a).[14] For a diblock copolymer, this depends on two main parameters, the A and B block volume fractions, f_A and f_B, where $f_A + f_B = 1$, and the segregation parameter χN, where N is the total degree of polymerization ($N = N_A + N_B$) and χ is the Flory–Huggins interaction parameter that varies inversely with temperature and specifies the degree of incompatibility between the A and B blocks (Figure 1-2b).[14] The correlation between χ_{AB} and temperature (T) is given by equation 1.[15,16]

$$\chi_{AB} = \left(\frac{z}{k_B T}\right)\left[\varepsilon_{AB} - \frac{1}{2}(\varepsilon_{AA} + \varepsilon_{BB})\right] \quad (1)$$

where z is a number of nearest neighbours per repeat unit in the polymer, k_B is the Boltzmann constant, k_BT is the thermal energy, ε_{AB}, ε_{AA}, and ε_{BB} are the interaction energies per repeat units of A–B, A–A, and B–B contacts, respectively.

a)

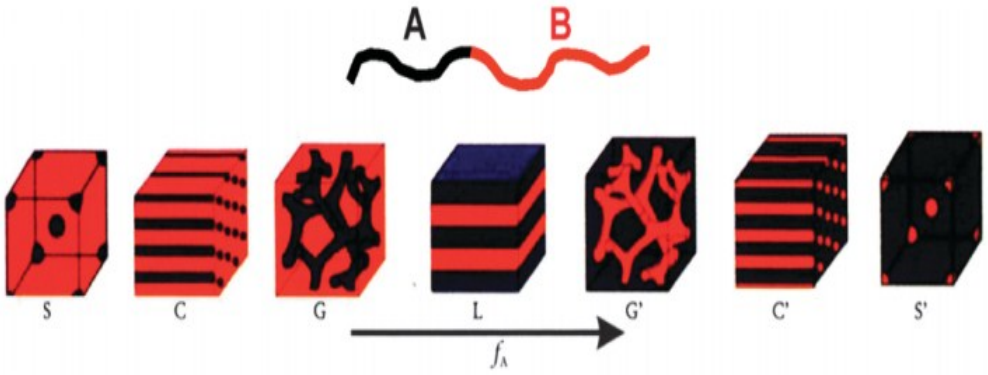

b)

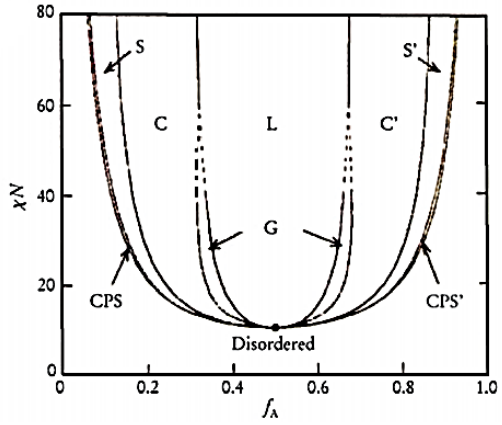

Figure 1-2. Microdomain phase separation of diblock copolymers in the bulk. a) Various morphologies of diblock copolymers as a function of the volume fraction, f_A, of the A block. b) Theoretical phase diagram of diblock copolymers in the bulk, predicted by the self-consistent mean field theory and the equilibrium morphologies as a function of f_A, and the segregation parameter, χN. Reproduced from ref. 15 with permission from The Royal Society of Chemistry.

Nano-objects obtained by block copolymer self-assembly, such as nanowires, nanorods and nanofibers, have a large variety of potential applications in electronic and optical devices. In addition, mesoporous materials, obtained by removing selected parts of the material (e.g. small molecules dissolved selectively in the minority phase) can be used as functional membranes in technological applications.[17-20] However, many other important applications require block copolymers to be assembled in the form of thin films.

1.1.2. Self-assembly in films

Films are often categorized as “thick” or “thin” (sometimes “ultrathin”). Thick films are generally of the order of micrometers or more in thickness, and block copolymer morphologies behave as in the bulk. They are often prepared by solvent casting. Thin films of block copolymers, which are generally less than 500 nm thick, are influenced not only by the same parameters as in the bulk, but also by the interfacial interactions of the blocks with the underlying substrate and of the free surface with air as well as by commensurability of the natural block copolymer periodicity and the film thickness.[12] They are typically prepared by spin-coating or dip-coating, sometimes followed by solvent annealing to obtain longer-range order. Ultrathin films sometimes have molecular-level thicknesses: this term applies, for example, to “monolayer” films prepared by the Langmuir-Blodgett technique, which is discussed in section 1.3. The list of potential applications of block copolymer thin films is long and continues to grow. Thanks to their two-dimensional order, they are widely used as nanotemplates in nanolithography, for the fabrication of ordered particle arrays and carbon nanotube arrays and as nanoporous membranes for virus filtration and drug delivery.[21-27]

1.1.3. Self-assembly in solution

When it comes to microphase separation of diblock copolymers in solution, the term "amphiphilic" is often used. Amphiphilicity is the ability to exhibit affinity to both hydrophilic and hydrophobic environments. However, this term can be applied not just to aqueous solutions, but also with respect to systems that comprise two incompatible solvents.[28] Besides the parameters, χ_{AB}, N, f_A and f_B, mentioned above, that govern the morphologies formed in the bulk, the presence of a solvent (S) introduces new Flory-Huggins interaction parameters. These are χ_{AS} and χ_{BS}, which describe the interactions between the solvent and each block.[29,30] When the solvent is compatible with both blocks (“neutral” solvent, χ of both blocks is below 0.5), the chains are molecularly dissolved. In contrast, if the solvent is highly

selective for one of the blocks and χ is above 0.5 for both blocks, micelle or vesicle formation occurs, depending on the volume fraction of the blocks. For example, when $\chi_{AS} >> \chi_{BS}$, the block copolymer chains form a micelle core from the insoluble block A and a corona from the soluble block B. Such block copolymer micelles are interesting analogues to surfactant micelles due to their high flexibility, high stability and ability to form a wide range of different molecular structures.[31]

The span of block copolymer applications in solution is broad. One of the most important areas of block copolymer use is for drug delivery. The micellar systems obtained by spontaneous assembly of block copolymers with well controlled and large variety of structure and functionality can be vehicles for different types of drugs. The hydrophobic-hydrophilic nature of block copolymers allows formation of complexes with drugs through non-covalent interactions with subsequent transportation to the target area. A wide range of studies have led to successful block copolymer-based drug delivery systems for anticancer drug therapy, delivery of DNA to the cells, and modification of drug pharmacokinetics that leads to increased efficiency of the drug used and decreased side effects. Another smart and not less important application of amphiphilic copolymers is sequestration in solution. For example, micelles formed from amphiphilic copolymers in aqueous solution can sequester hydrophobic compounds in their hydrophobic interior. This allows such systems to be used for the extraction of organic molecules as well as organic solvents.[28]

1.2. Amphiphilic diblock copolymers of PS-P4VP and supramolecular PS-P4VP complexes

The first and the main advantages of supramolecular complexes include the ease of small molecule substitution and obtaining new functional materials instead of synthesizing new ones.[32,33]

Polystyrene-poly(4-vinyl pyridine) (PS-P4VP) diblock copolymers have often been chosen for studies of self-assembling systems due to the wide variety of compositions that are commercially available and because the P4VP block can be

modified by protonation, quaternization and coordination chemistry (all forms of supramolecular chemistry). Earlier studies focused on the behaviour in the bulk.[34-36] Morphology control in thin films of PS-P4VP systems has been a subject of more recent investigations.[37-40]

In general PS-P4VP is an amphiphilic block copolymer, where PS is the hydrophobic part and P4VP is the hydrophilic part. A variety of different structures in the bulk and in thin films can be obtained by changing conditions, such as the nature of the solvent, fraction of blocks in the copolymer, experimental conditions such as temperature, compression force, compression rate, *etc*. Some specific examples are given below.

The addition of block-selective small molecules to block copolymers, leading to the formation of supramolecular complexes, is an effective way of producing self-assembled structures with tunable morphologies. A commonly used strategy is to add hydrogen-bonding small molecules to a diblock copolymer with one block that is a hydrogen bond acceptor. This has been studied most frequently with PS-P4VP. The block selectivity results in an increase in the volume fraction of the P4VP phase that leads to the morphological transformations.[37] Ikkala, ten Brinke and coworkers were among the leaders who established the basic principles of construction of supramolecular block copolymers in the bulk by the attachment of small molecules via different types of interactions, such as electrostatic interactions, metal coordination and, especially, hydrogen bonding. [20,36,20,41-42]

Frequently used small molecules for supramolecular complexes with PS-P4VP are 3-*n*-pentadecylphenol (PDP) and 2-(4′-hydroxybenzeneazo)benzoic acid (HABA). Ikkala, ten Brinke and coworkers and Tung and coworkers used PDP and demonstrated the possibility of obtaining structure-within-structure morphologies (Figure 1-3).[43-46] This results from the repulsion between the polar P4VP backbone and the nonpolar alkyl chain of PDP (and other similar molecules) that causes nanophase separation, leading to a liquid crystalline lamellar structure within the P4VP-based phase. Stamm and coworkers privileged HABA to achieve morphological transformations in different PS-P4VP diblock compositions and varying P4VP/HABA molar ratios, often combined with solvent annealing.[47]

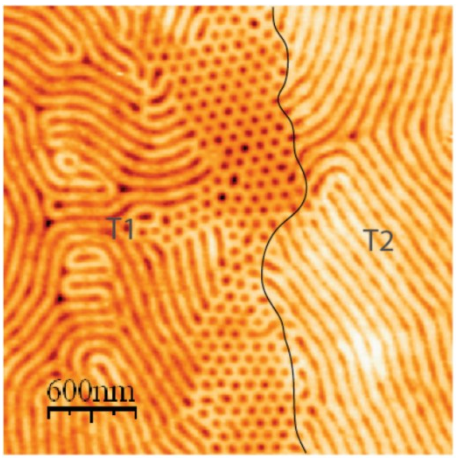

Figure 1-3. Transition between lamellae and perpendicular cylinders structure in dip-coated film PS(252k)-P4VP(43k)/PDP occurred after 17 h of chloroform vapour annealing at high pressure. T1 and T2 are different terraces of the film. Reprinted with permission from ref. 47. Copyright 2008 American Chemical

Roland *et al.* investigated dip-coated films prepared from THF solutions of PS-P4VP with naphthol (NOH) or naphthoic acid (NCOOH), which differ only in their functional hydrogen-bonding substituent.[39,48-49] They showed that film thickness varies in a V-shaped manner with dip-coating rate and that the small molecule uptake during dip-coating increases with dip-coating rate, starting from a low value, in the same way for both small molecules. For the system studied, where the solution composition of small molecule to 4VP repeat units was equimolar, the film morphology evolved from dots (spherical morphology) to stripes (cylindrical morphology, with cylinders parallel to the substrate) for NOH and from dots to stripes to face-down lamellae for NCOOH.

1.3. Langmuir-Blodgett and Langmuir-Schaefer techniques (ultrathin films)

1.3.1. Some historical aspects

An ancestor to the Langmuir trough and Langmuir-Blodgett technique was developed by Agnes Pockels in the 1890's. She was the first to measure the surface

tension of monolayers on water in her own kitchen using household materials.[50] Irving Langmuir improved on Pockel's trough, and determined the main properties of organic monolayer films on liquids, published in 1917.[51] In 1918 he began to collaborate with Katharine Blodgett, who soon realized that multilayer films can be easily fabricated by multiple dipping of a solid substrate into water covered by a monolayer of suitable organic molecules. In the first such experiment, a calcium stearate monolayer was transferred from the water surface to a glass substrate. A practical use for such films as an antireflective coating was later suggested.[52] Since then, the Langmuir-Blodgett (LB) technique has received considerable attention for a wide range of scientific investigations involving surfaces, although large-scale practical applications are still limited.

1.3.2. Langmuir isotherms

The Langmuir isotherm is based on measuring the surface tension. Pure water has a very high surface tension, around 73 mN/m at 20°C, due to the multiple hydrogen-bonding interactions among H_2O molecules. The introduction of impurities reduces the surface tension, leading to a change in the surface free energy of water (air/water interface). The surface pressure (π) can be calculated from the difference between the surface tension of pure water (γ_0) and the surface tension after addition of a substance that adsorbs to the water surface (γ) (equation 2).[53,54]

$$\pi = \gamma_0 - \gamma \qquad (2)$$

By measuring π during compression of the total surface area, one obtains the Langmuir compression isotherm. This isotherm provides qualitative and quantitative information about the self-assembly and the formation of a thin monolayer film on the surface. In different regions of the isotherm, the orientation of amphiphilic molecules at the air/water interface can be deduced.

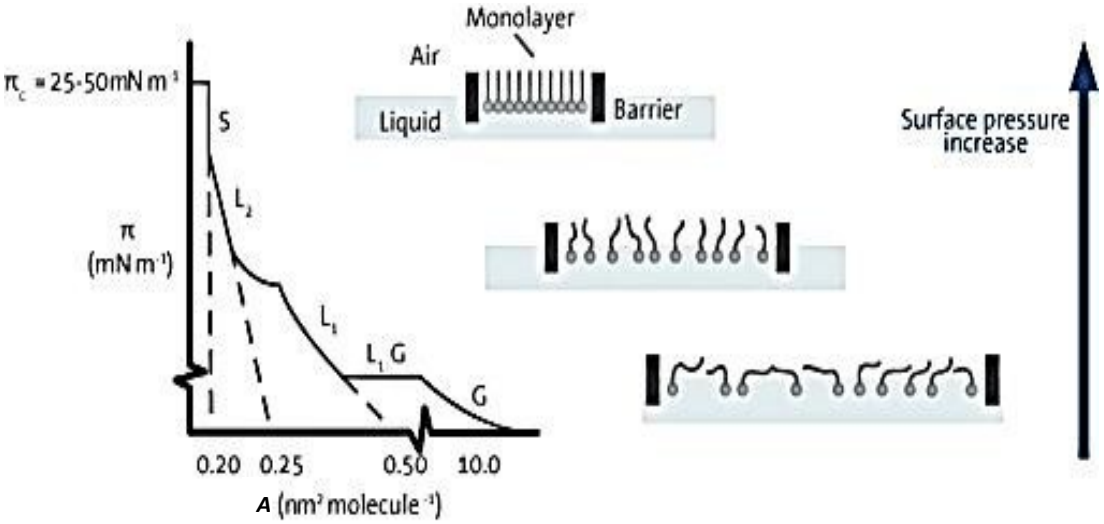

Figure 1-4. Langmuir-Blodgett compression isotherm of a phospholipid showing different phases: G – gaseous, L_1 – liquid expanded, L_2 – liquid condensed, S – solid. Used with permission from Biolin Scientific.

Figure 1-4 shows a typical isotherm of the extensively studied phospholipid monolayer, obtained by measuring the surface pressure (π) of the interfacial film as a function of the mean molecular area (A) of the compound spread at the air/water interface. In a typical experiment, a very small amount of the amphiphilic substance is spread on the water surface, so that the molecules are far enough apart from each other that the interactions among them are essentially absent. This monolayer can be considered to be a two-dimensional gas because of the large average intermolecular distance. In this case, it does not have a significant effect on the free energy of the subphase and the surface pressure is very low (< 0.5 mN/m). During compression of the surface area, the molecules become closer to one another and phase transformations analogous to the phase transitions between the three-dimensional gaseous, liquid and solid states, can take place. Thus, the isotherm is the 2D equivalent of what is obtained when plotting the pressure vs volume (at constant temperature) of a material being compressed. In the first transition, from

gas to liquid state, the hydrocarbon chains start to lift away from the air/water interface, and the liquid-expanded state is formed. In this state, the hydrocarbon chains are randomly oriented. At the liquid-expanded/liquid-condensed transition, condensed domains appear in the expanded phase. This LE/LC phase coexistence typically manifests itself as a region of constant or quasi-constant surface pressure, called isotherm plateau, and is a characteristic of a first order thermodynamic transition. The liquid-condensed phase can be followed by a transition to a solid phase of closely packed molecules. In this phase, the hydrocarbon chains are crystallized and uniformly oriented, and the monolayer presents a strong lateral cohesion. At still further compression, the monolayer will collapse into a three-dimensional structure and often disordered multilayers will be formed.[55]

1.3.3. Langmuir-Blodgett (LB) and Langmuir-Schaefer (LS) techniques

To form a Langmuir film, it is necessary to have a water insoluble substance that is soluble in a volatile solvent. Such materials usually consist of two parts, a "head" and a "tail". The "head" part is hydrophilic, with a strong dipole moment. The "tail" is hydrophobic and is typically composed of a long aliphatic chain, as in the fatty acids. Such molecules, having distinct hydrophobic and hydrophilic regions, are called amphiphiles. (Figure 1-5b).[56] The following preparation steps are necessary: solubilizing the substance of interest in a volatile organic solvent (chloroform, toluene, hexane, *etc.*) that does not dissolve in or react with the subphase, uniformly spreading this solution onto the water surface of the Langmuir trough, allowing for evaporation of the solvent, and compressing the barriers

a) 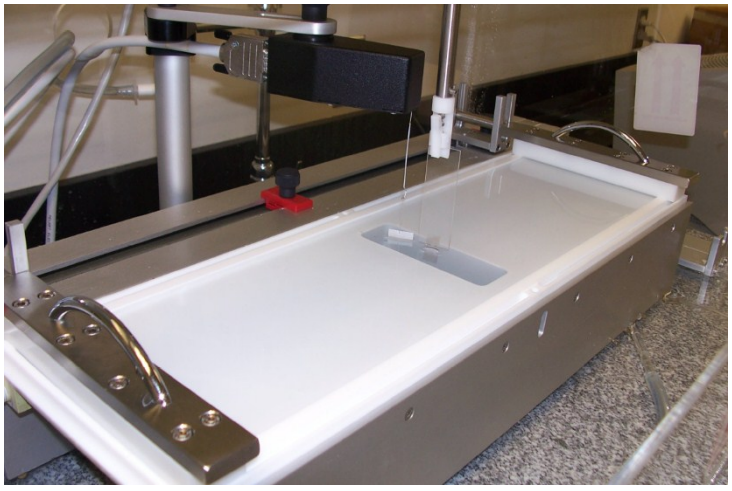 b) 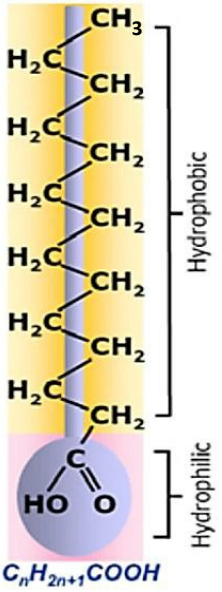

Figure 1-5. a) Langmuir trough (KSV 3000). b) The chemical structure of a typical LB compatible molecule with an aliphatic tail and a carboxylic acid head. Image *b* used with permission from ref. 58.

The Langmuir-Blodgett trough that is used in this thesis is shown in Figure 1-5a. It consists of a Teflon container for the liquid (water) subphase, moveable barriers for compressing the surface area and devices for measuring the surface pressure and for transferring the monolayer to a solid substrate.[57]

The term, "Langmuir–Blodgett film", refers to a monolayer or a multilayer of an organic material that has been transferred from the water surface to a solid substrate such as mica, silicon, glass or quartz, by vertical deposition. In this case, the vertically oriented substrate is dipped and pulled through the monolayer at the air/water interface one or more times until the desired number of layers has been deposited (Figure 1-6).[56]

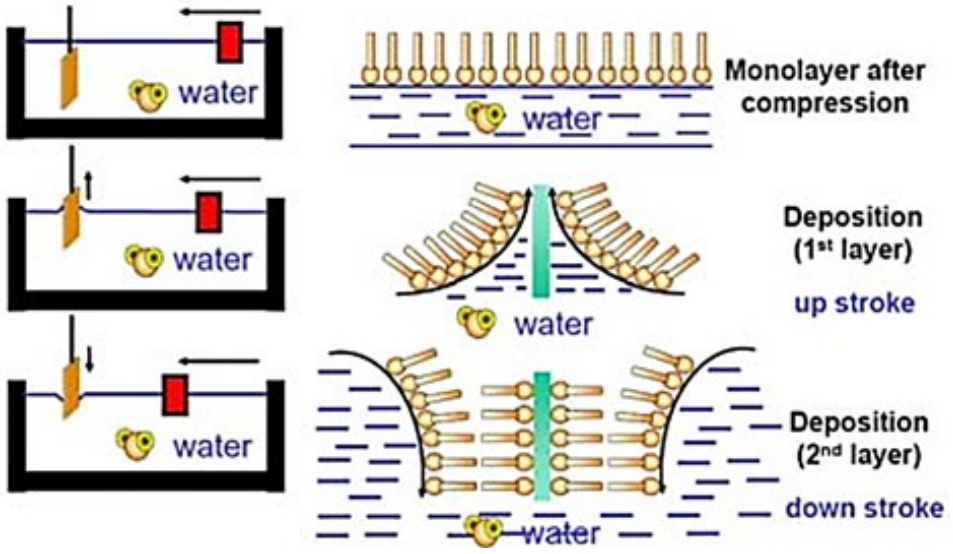

Figure 1-6. Langmuir-Blodgett deposition of monolayers from the water surface to a solid substrate. Image used with permission from ref. 58.

Usually, deposition is done at a constant surface pressure and at a constant transfer rate (1-5 mm/min). The film adsorbs to the substrate through hydrophilic/hydrophobic interactions and is characterised by the deposition (transfer) ratio.[56] This transfer ratio is calculated from the decrease in the area occupied by the monolayer during the transfer divided by the coated area of the substrate. A transfer ratio close to or equal to one indicates a high-fidelity deposition and the orientation and organisation of the molecules on the substrate should be the same as on the water surface.[58] A transfer ratio higher than one can occur if there is microscopic inhomogeneity at the substrate surface. A transfer ratio lower than 0.8 indicates poor homogeneity of the deposited film and a possible change in the molecular orientation during the deposition process.[55]

Another (less used) technique for depositing Langmuir films is the Langmuir-Schaefer method. In this case, as shown in Figure 1-7, the substrate touches the monolayer on the water surface horizontally and lifts it up from the top[59] (Figure 1-7a) or, alternatively, it is submerged in the subphase and the monolayer is lifted up from the bottom (or the water level is lowered, which has the same effect) (Figure 1-7b).[60] This technique minimizes the stress and deformation

problems associated the Langmuir-Blodgett transfer, but calculation of a transfer ratio in this method is problematic.[59]

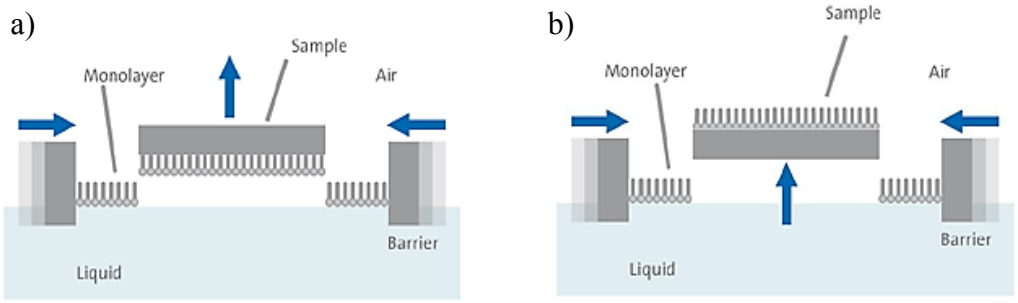

Figure 1-7. Two different types of Langmuir-Schaefer deposition. Used with permission from Biolin Scientific.

1.4. Infrared spectroscopy

Infrared (IR) spectroscopy is a type of vibrational spectroscopy frequently used due to its ability to analyse samples in all states. The IR spectroscopy technique is based on the vibrations of atoms in a molecule. The main concept of this method is to pass infrared radiation through the sample and measure what portion of the incident radiation is absorbed at a specific energy, normally expressed in wavenumbers. The energy of the bands appearing in the absorption spectrum corresponds to the vibration frequency of specific molecular groups in the sample. Analysis of IR spectra can give information about the type of molecules present in a sample, their relative quantities, their molecular structure and their molecular environment.

The history of IR spectroscopy started in 1940 when the first IR spectrometers based on prisms as dispersive elements became available commercially. Later, diffraction gratings were incorporated as the dispersion mechanism. A leap forward was made with the development of Fourier transform spectrometers. The quality of spectra was significantly increased, along with a decreased time for obtaining the data.[61]

FTIR have many advantages compared to other types of infrared spectrometers. The first and main advantage is the possibility to measure IR spectra with a high signal-to-noise ratio (SNR), including for challenging samples such as Langmuir monolayers. The high SNR is possible due to the throughput advantage of FTIRs, which reflects the amount of light reaching the detector compared to the input light. Due to the specifics of the instrument (in particular the absence of entrance and exit slits that reduce throughput), a high-intensity IR beam reaches the detector and increases the signal level. The SNR improves as:

$$\mathrm{SNR} \propto t^{1/2} \propto N^{1/2} \tag{4}$$

where t is the observation time, which is characterized by the number of coadded scans N. It is obvious that increasing of the number of scans improves the SNR, which in turn leads to improving the spectrum quality in general. The second advantage of FTIR, the multiplex advantage, leads to an improvement of the SNR as in equation 5:

$$\mathrm{SNR} \propto n^{1/2} \tag{5}$$

where n is the number of resolution elements in the spectrum.

Another advantage of FTIR is the wavenumber precision. FTIR allows the measurement of wavenumbers, and hence band positions, reproducibly, with a precision of better than ±0.01 cm^{-1}.[62] This will prove especially useful in our study of molecular interactions in LB films of PS-P4VP complexes with PDP.

The transmission method is historically the most frequently used sampling approach in FTIR due to the inexpensive sample preparation procedure, wide range of samples that can be analyzed and the good signal-to-noise ratio. It is based on the absorption of IR light at specific wavenumbers when it passes through the sample. This is the almost universal technique. It is, however, quite challenging to analyze ultrathin films by transmission FTIR due to the extremely short pathlength and,

thus, low absorbance of these samples.[62] In that case, the multiple reflection ATR-IR technique can be used to improve the SNR of the spectra.

1.4.1. General principles of ATR-IR

ATR-IR is an infrared spectroscopy technique based on the principle of attenuated total reflection (ATR). This technique has many advantages, such as an easy sample preparation (if any) and analysis, great sampling flexibility for analyzing a variety of samples (including ultrathin films), high surface sensitivity, and the possibility of qualitative and quantitative analysis of molecular composition, structure, and even 3D orientation.

In general, ATR is a surface sensitive analytical technique based on the phenomenon of total internal reflection. The beam of infrared light passes through the ATR crystal and is totally reflected at the crystal/sample interface (Figure 1-8). However, the reflected beam forms an evanescent wave at the interface which penetrates inside the sample. The penetration depth (DP) is usually between 0.5 and 3 micrometers and is calculated by equation 6:

$$DP = 1/[2\pi W n_c(\sin^2\Phi - n^2_{sc})^{1/2}] \quad (6)$$

where W is the wavenumber, n_c is the refractive index of the ATR crystal, Φ is the angle of incidence, and n_{sc} is the ratio of the refractive indices of the sample and ATR crystal. In the case of ultrathin films, the refractive index of the sample is usually replaced by the refractive index of air.

The number of ATR reflections depends on the angle of incidence of light and on the geometry of the crystal. If the user is interested only in qualitative analysis or in the quantitative analysis of thick samples, one reflection is usually enough. Single-bounce ATR accessories are now widely available and commonly used instead of transmission. Multiple reflections are often necessary in the case of quantitative analyses on ultra-thin films or diluted solution. This multiplies the sample absorbance by the number of reflections and thereby increases the

sensitivity of ATR detection. After one or more reflections, the light beam exits the crystal and travels to the detector (Figure 1-8).[62]

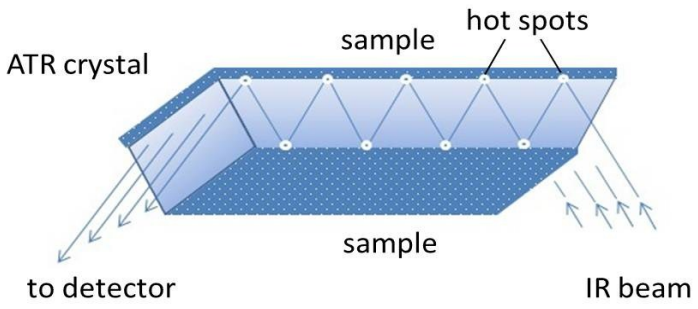

Figure 1-8. The principle of attenuated total reflection. The circles denote the "hot spots" where the evanescent wave interacts with the sample.

The refractive index of the ATR crystal must always be greater than the refractive index of the sample; otherwise the light can refract into the sample and lead to spectral distortions. Equation 6 shows that when the refractive index of the crystal increases, the penetration depth decreases. Thus, by changing the ATR crystal, the penetration depth can be changed easily and the spectra of a substance at different depths can be obtained. In the context of ultrathin films, it is advantageous to use a high refractive index crystal, such as silicon or germanium, to optimize the interaction of the IR electric field with the sample. Besides refractive index, other properties of the crystal, such as surface wettability, durability, toughness, useful wavenumber range and pH sensitivity, are important.[62]

1.4.2. Determination of orientation by ATR-IR

Polarized ATR-IR can be used for the determination of molecular orientation in a sample. Orientation provides the anisotropic macroscopic physical properties of materials. The accurate quantification and interpretation of molecular orientation give detailed information about the molecular structure of materials and can lead to improvements in technological processes.[63]

The orientation of molecular vectors, such as the molecular axis C or the transition dipole moment M, can be defined with respect to a Cartesian coordinate system (X, Y, Z) by defining the average angles between the vectors and the reference directions. Ultrathin films usually present a uniaxial orientation with respect to the normal of the substrate (Z axis) and thus an isotropic distribution of C and M in the plane (X, Y) of the film. It is therefore sufficient to discuss the orientation in the system as a cone distribution of M about the molecular axis C (with an average β angle), which is itself distributed around the reference direction Z with an average θ angle, as represented in Figure 1-9.

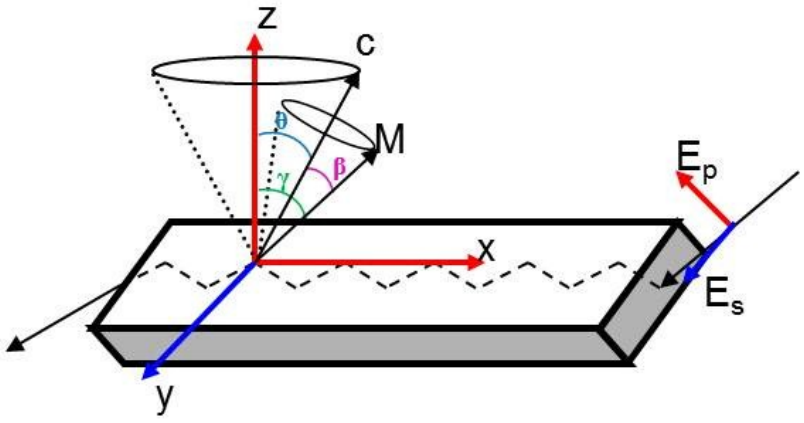

Figure 1-9. Schematic of the uniaxial orientation in an ultrathin film measured by polarized ATR. The molecular axis C is oriented uniaxially at an average angle θ with respect to the normal of the substrate, Z, while the transition dipole moment, *M*, is uniaxially oriented at an average angle β with respect to C. E_P and E_S represent the polarization of the electric field of the incoming IR light, and γ is the average angle between the dipole moment *M* and the reference direction Z.

The molecular orientation is expressed by the $<P_2>$ coefficient, the order parameter. At a $<P_2>$ value of 0, there is no molecular orientation with respect to Z and the sample is completely isotropic. For $<P_2>$ values between 0 and 1, there is orientation parallel to Z axis. Negative values between 0 and -0.5 indicate an orientation perpendicular to the Z axis.[64]

A molecular order parameter is usually calculated in three steps.[65,66] The absorbance of the oriented sample strongly depends on the polarization of the incident radiation, the so-called linear dichroism, which can be measured by recording an IR spectrum using light that is polarized parallel and perpendicular to a reference direction. In the case of ATR, the reference direction is defined by the plane of incidence of the IR radiation in the ATR crystal. The degree of optical anisotropy is characterized by the dichroic ratio (R), which is the first step of calculation:

$$R = \frac{A_p}{A_s} \tag{7}$$

where A_P and A_S are the absorbance with parallel and perpendicular polarized radiation, respectively.[67]

When R is known, it is possible to calculate the order parameter, $S_z = < P_2(\cos\gamma) >$, which defines the orientation of the transition dipole moment M of the band of interest with respect to the normal of ATR crystal (Z axis). In contrast to the case of polarized transmission measurements, for which R can be directly converted into the order parameter, polarized ATR measurements require knowledge about the intensity of the electric field along the three main axes (X, Y and Z). The following equation can be applied:[65]

$$S_z = \frac{<E_x^2> - <E_y^2> \cdot R + <E_z^2>}{<E_x^2> - <E_y^2> \cdot R - 2 \cdot <E_z^2>} \tag{8}$$

where $< E_x^2 >, < E_y^2 >, < E_z^2 >$ are the mean square electric field (MSEF) amplitudes of the evanescent polarized radiation in the film. For LB films, these MSEF amplitudes can be reliably calculated using the Harrick approximation for ultrathin films:[68]

$$< E_x^2 > = \frac{4\cos^2\Phi_1(\sin^2\Phi_1 - n_{31}^2)}{(1 - n_{31}^2)[(1 + n_{31}^2)\sin^2\Phi_1 - n_{31}^2]} \quad (9)$$

$$< E_y^2 > = \frac{4\cos^2\Phi_1}{(1 - n_{31}^2)} \quad (10)$$

$$< E_z^2 > = \frac{4\, n_{32}^4 \cos^2\Phi_1 \sin^2\Phi_1}{(1 - n_{31}^2)[(1 + n_{31}^2)\sin^2\Phi_1 - n_{31}^2]} \quad (11)$$

where $n_{31} = n_3/n_1$, $n_{32} = n_3/n_2$, Φ is the incident angle, and 1, 2 and 3 refer to the ATR crystal, the sample and the medium (air), respectively.

The last step is the calculation of the molecular order parameter S_m. Assuming cylindrical symmetry of the transition dipole moments relative to the molecular axis C, $S_m = <P_2(\cos\theta)>$ can be calculated using the Legendre addition theorem (equation 12):

$$< P_2(\cos\theta) > = \frac{3 \cdot <\cos^2\theta> - 1}{2} = \frac{S_z}{<P_2(\cos\beta)>} \quad (12)$$

where θ is the angle between the molecular axis C and the reference direction Z, and β is the angle between the transition dipole moment and the molecular axis. Considering that the angle β is generally fixed, the orientation distribution of *M* around C is narrow and $< P_2\ (\cos\beta) > = P_2\ (\cos\beta)$.

1.5. Previous investigations of morphology formation in LB diblock copolymer films

Self-assembly of amphiphilic diblock copolymers at the air/water interface and in LB films has been investigated by various groups.[69-71] Generally, three main types of morphologies are obtained, depending on the selective block length: a) planar-type aggregates (also called pancakes or islands), which are variable in size and appear at low hydrophilic block content; b) nanostrands (also called spaghetti, cylinders, worms, strands) of variable length and often interconnected leading to the formation of a nanostrand network,[72,73] for somewhat higher hydrophilic block content; and c) dots (or nanodots) that are more uniform in size and have a tendency to assemble into an ordered two-dimensional array (usually hexagonal, but sometimes square[74]) at still higher hydrophilic block content (Figure 1-10).

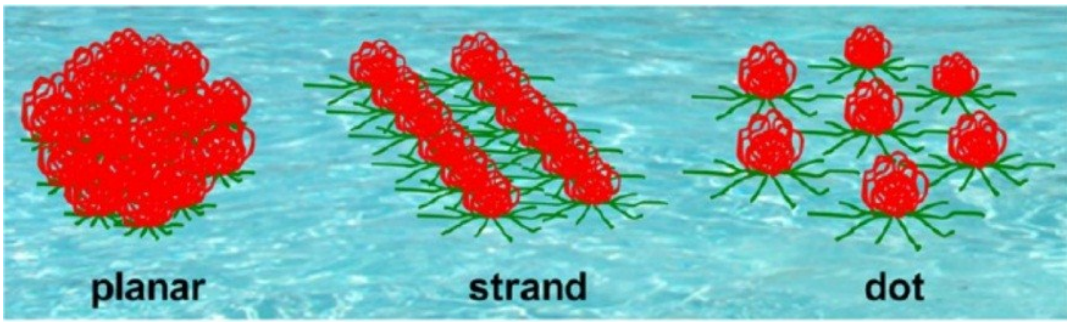

Figure 1-10. Schematic image of the main morphology types in LB monolayers of amphiphilic diblock copolymers. Red features represent hydrophobic blocks, green features hydrophilic blocks. Reprinted with permission from ref. 73. Copyright 2013 American Chemical Society.

Of the three morphologies, just a nanodot morphology shows a well-defined transition in the Langmuir isotherm. This is observed as a plateau, as shown in Figure 1-11 for the PS-P4VP(29.4%)/PDP system investigated in our group in recent years.[74]

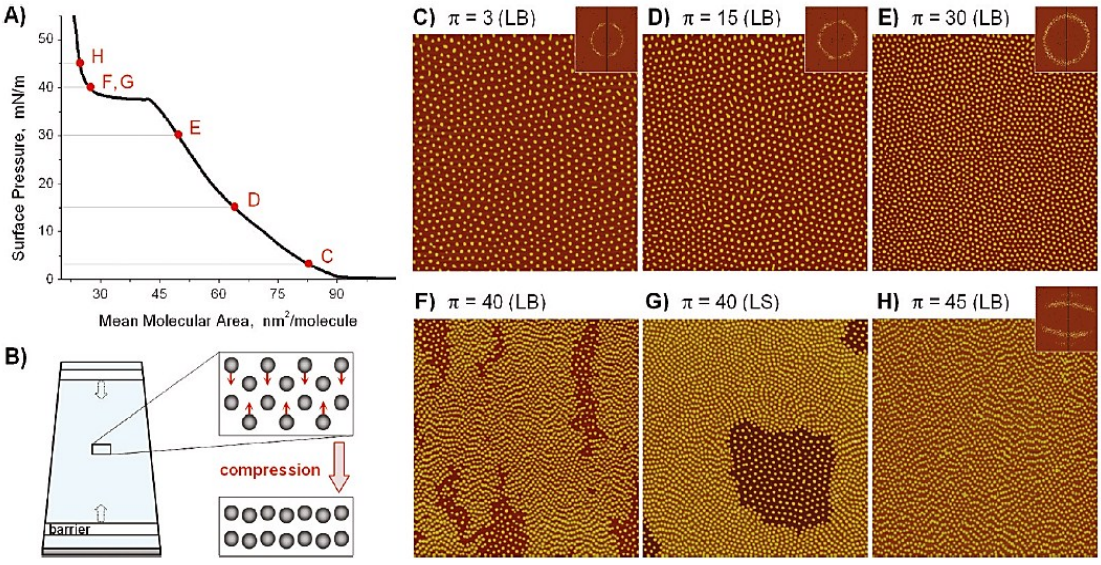

Figure 1-11. (A) Langmuir compression isotherm of PS-P4VP(29%)/PDP at the air/water interface. (B) Model of order-order transition as a result of barrier compression. The image illustrates a Langmuir trough (arrows show direction of barrier compression) and the nanodot morphology below (top, with red arrows indicating dot movement upon compression) and above (bottom) the plateau pressure. (C-H) AFM height images (5 x 5 μm^2) of Langmuir-Blodgett (LB, in C-H) and Langmuir-Schaefer (LS, in G) monolayer films transferred at the surface pressures (π) indicated. Corresponding 2D FFTs are given in the upper right corner for C-E and H. The direction of transfer (for C-F and H), coincident with the barrier compression direction (for C-H, including G), is along the Y-axis. Reprinted with permission from ref. 76. Copyright 2011 American Chemical Society.

In accordance with surface pressure rules, such a plateau is indicative of a pressure-induced first-order phase transition.[69] This transition had previously been interpreted as a "starfish → jellyfish" transition. In this case, the surface-adsorbed hydrophilic blocks ("starfish") at low compression become submerged into the water ("jellyfish") at the transition pressure.[75] However, later investigations refuted this hypothesis, at least for PS-P4VP derivatives where the P4VP block is quaternized with variable-length alkyl chains, since no significant thickening of the

ionic layer was observed at pressures above the transition by *in situ* X-ray and neutron reflectivity experiments.[76] On the other hand, *in situ* FTIR showed an increase in the trans conformation of long alkyl chains with increased pressure, suggesting a disorder-order change of the alkyl side chains.[76] However, the same transition is observed in diblock copolymers without alkyl chains, such as PS-PEO[77] and PS-P4VP[74]. This indicates, that the transition must involve a more general mechanism than one based on alkyl chain changes.

Our group recently found, using PS-P4VP(29.4%)/PDP that the morphological order of the nanodots changes at the transition, going from hexagonal-like order to square-like order at the plateau pressure (Figure 1-11). The structure of LB films of this PS-P4VP diblock copolymer complex with PDP has a different type of morphology for the parts of the LB isotherm below and above the plateau. The hexagonally ordered dot morphology observed at low surface pressure (before the plateau region, Figure 1-12, a) changes to square-like order at high surface pressure, with a mix of hexagonal and square-like order within or just above the plateau (Figure 1-12, b). The appearance of the square-like structure was thought to be the result of pushing the rows of dots toward each other under high surface pressure. The height of the dots remains approximately constant during the transition. The increase in background height by about 3 nm, indicated by the lighter colour of the background compared to the darker colour (Figure 1-12, b) was associated to a possible change of the orientation of PDP molecules. Considering that the length of the PDP molecule is 2.6 nm, the increase in the background height can be interpreted as a result of changing the orientation of PDP molecules from prone to almost perpendicular relative to the surface. The schematic model of such molecular reorientation is presented in Figure 1-12, c-d. However, this interpretation has not yet be proven, which might be possible to do by an infrared spectroscopic study.

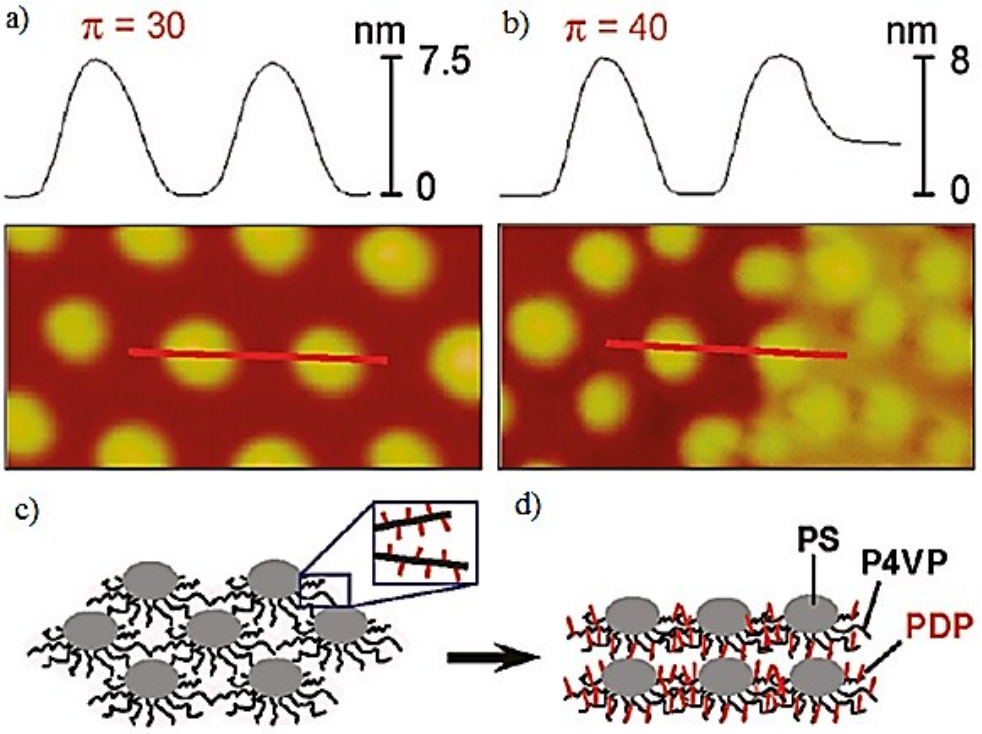

Figure 1-12. Height profiles of AFM images (500 x 250 nm^2) of LB films transferred at 30 and 40 mN/m respectively. (c-d) Model illustrating the changes that occur at the plateau transition: nanodot reorganisation accompanied by alkyl chain (red lines) reorientation from prone to vertical. Reprinted with permission from ref. 76. Copyright 2011 American Chemical Society.

1.6. Objectives and structure of the thesis

The current work is based on the recent discovery of the order-order morphological transition of amphiphilic diblock copolymers at the air/water interface, as summarized in the previous section.[74] The project can be divided into two parts. The first objective is to extend the previous studies involving PS-P4VP/PDP to related systems, particularly to PS-P4VP complexed with naphthol (NOH) and naphthoic acid (NCOOH), which were used by Roland *et al.* for dip-coated thin films.[39] The second objective is to improve our understanding of molecular-level changes that must underlie or accompany the order-order transition occurring at the isotherm plateau pressure. This part of the study involves highly challenging ATR-IR investigations of monolayer films, and was accomplished with the close collaboration of Marie Richard-Lacroix.

The thesis is presented in 4 chapters:

Chapter 1 contains general information about the self-assembly of block copolymers and the formation of thin films by different methods. The main concepts of ATR-IR and its use for quantifying molecular orientation are also presented as well as the objectives of the thesis.

Chapter 2 presents the experimental procedures; i.e. sample preparation, the AFM method used to image the morphologies, details related to ATR-IR, etc.

Chapter 3 in the first part gives the results obtained for LB and LS films of PS-P4VP complexed with naphthol and naphthoic acid. In particular, the influence of solution concentration and surface pressure is investigated. The second part confirms the order-order transition in LB and LS films of PS-P4VP and PS-P4VP/PDP using AFM and presents the results of ATR-IR analysis of the films. The latter required much time to find the appropriate conditions (cleanliness of water surface and substrate, determination of best substrate, substrate preparation,

type of IR technique, rapidity of measurement relative to sample preparation, etc.) for obtaining analyzable spectra.

Chapter 4 summarizes the main results and conclusions obtained from the thesis work and proposes ideas for future research.

CHAPTER 2

EXPERIMENTAL DETAILS

2.1. Materials

Two polystyrene-*b*-poly(4-vinyl pyridine) (PS-P4VP) block copolymers were obtained from Polymer Source (Montreal, Canada) and used as received:

- PS-P4VP with M_n (PS) = 20,000 g/mol, M_n (P4VP) = 17,000 g/mol (192 S repeat units, 162 VP repeat units, 46 mol % P4VP content); referred to as PS-P4VP (46%)
- PS-P4VP with M_n (PS) = 36,500 g/mol, M_n (P4VP) = 16,000 g/mol (350 S repeat units, 152 VP repeat units, 30.3 mol % P4VP content) ; referred to as PS-P4VP (30.3%)

The small molecules used were 1-naphthol (NOH) (Sigma-Aldrich, 99%; used as received), 1-naphthoic acid (NCOOH) (Fluka, 97%; used as received), 3-*n*-pentadecylphenol (PDP) (Sigma-Aldrich, 90%; recrystallized twice from hexane before use). The molecular structure of PS-P4VP and the small molecules used are presented in Figure 2-1.

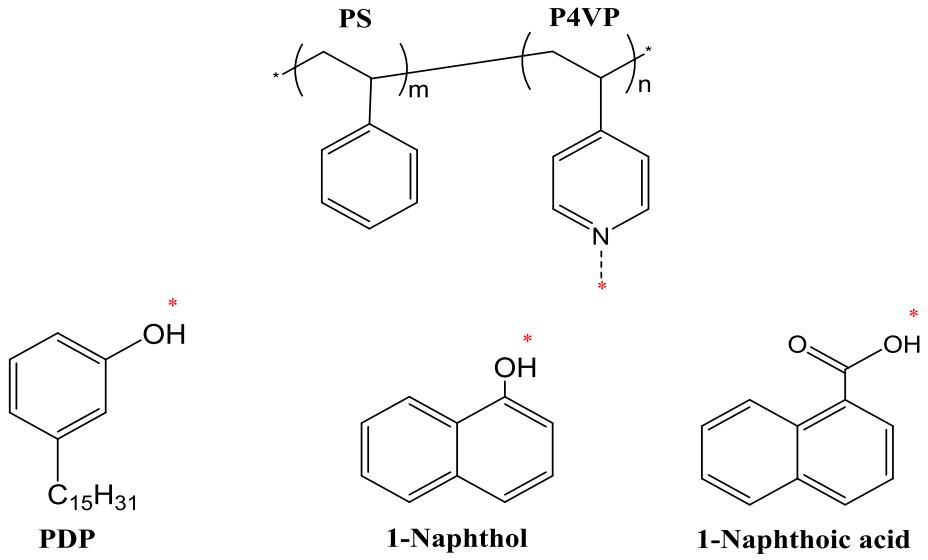

Figure 2-1. Molecular structure of PS-P4VP and the small molecules used. The red stars indicate the hydrogen-bonding sites.

Chloroform (Sigma-Aldrich, HPLC grade, ≥99.8% or EMD Millipore, HPLC grade, ≥99.8%) was used as the solvent for solution preparation, cleaning of

the ATR crystal and, together with anhydrous ethanol (Commercial Alcohols), in all Langmuir-Blodgett trough cleaning processes. Ultrapure water (18.2 MΩ.cm), obtained by the purification of distilled water with a Milli-Q Gradient system, was used as the subphase in the Langmuir-Blodgett trough. Muscovite ruby mica (Hi-Grade Mica, Grade V2, Ted Pella Inc., Redding, USA), silicon wafers (University Wafer, type P, Boston, USA), and Si and Ge crystals (parallelepiped-shaped with truncated 45º side edges, 52 x 20 x 2 mm, surface quality 40/42 scr/dig for Si and 60/40 for Ge, Tydex, St. Petersburg, Russia) were used as solid substrates for LB and LS depositions and further analysis.

The substrates were cleaned as follows. Mica was cleaved immediately before use. The silicon wafers were cleaned by a Piranha solution (3:1 v/v mixture of concentrated H_2SO_4 and 30% H_2O_2). The Ge and Si ATR crystals were cleaned with HPLC chloroform and anhydrous ethanol followed by oxygen plasma cleaning (5 min, Plasma Cleaner/Sterilizer PDC-32G, Harrick Plasma, NY, USA) before deposition.

Mica substrates and, to a lesser extent, silicon wafers, are typically used for LB and LS deposition and subsequent AFM investigation of ultrathin film morphology. Thus, the first ATR experiments were done on silicon wafer substrates (mica substrates are not suitable because of their strong absorption throughout the IR region) immediately after sample deposition; but, due to the very small thickness of the film, the signal was too weak for quantitative analysis. It was then proposed to transfer samples directly on 24-reflection Ge crystals, freshly cleaned with HPLC chloroform and anhydrous ethanol before deposition, in the hope of increasing the signal intensity. However, a problem of low transfer ratios onto the Ge substrates was found. The cleaning procedure was modified to include an oxygen plasma cleaning step to make the surface of the ATR crystal more hydrophilic (water contact angle of 0º), but the results were still poorly reproducible. We believe that the reason for the low transfer ratio is poor affinity between the Ge substrate and the sample. Finally, it was found that use of a 24-reflection Si ATR crystal for the LB transfers led to good results. A high transfer ratio was obtained for these Si crystal substrates, which were cleaned by the same procedure as for Ge crystals

(except for pure PS-P4VP at higher surface pressures). Qualitative and quantitative information was extracted from the spectral range above 1500 cm^{-1}, since silicon dioxide absorption becomes problematic at lower wavenumbers.

2.2. Methods

2.2.1. Solution and sample preparation. Langmuir-Blodgett and Langmuir-Schaefer films

To prepare the solutions used for spreading at the air/water interface, PS-P4VP was dissolved in $CHCl_3$ and then an appropriate amount of the desired small molecule (SM) was added (1.0:1.0 VP:SM molar ratio). The solution was left to stir overnight at room temperature in a sealed volumetric flask. The final solution concentration of PS-P4VP varied between 0.1 and 5 mg/mL.

A computer-controlled Langmuir-Blodgett system (KSV 3000, KSV Instruments, Helsinki, Finland) with a platinum Wilhelmy plate sensing device was used. The trough was cleaned with $CHCl_3$ and ethanol and then it was filled with MilliQ water. The temperature of the subphase in the trough was maintained at 20-21ºC using a refrigerated circulator (Isotemp 3016, Fisher Scientific). Before each experiment, a blank compression was performed to verify the cleanliness of the water surface. The solution was spread on the water surface with the barriers completely open using a Hamilton microliter syringe of the desired volume (20-100 μL for concentrated solutions, 40-400 μL for dilute solutions) in staggered rows. It is very important to follow the same way of spreading for each experiment and to deposit at least one drop at 3-4 cm from the immersed substrate for optimal reproducibility. After spreading, the solvent ($CHCl_3$) was left to evaporate for 30 min. To obtain Langmuir isotherms of the surface pressure (π) as a function of the mean molecular area (A), the barriers were compressed symmetrically at a constant rate of 10 mm/min (15 cm^2/min). Each isotherm was repeated at least twice, often three times. To deposit monolayers using the LB technique, the barriers were compressed to the desired surface pressure and then held in place for 20-30 min to allow barrier position and surface pressure stabilization. The monolayer was then

transferred vertically by raising at a fixed withdrawal rate (5 mm/min) a solid substrate that had been submerged in the subphase prior to spreading the polymer solution. The transfer ratio of the deposited films was generally 1.0 ± 0.2. Langmuir-Schaefer (LS) films were transferred horizontally onto a solid substrate (mica or silicon wafer) that was fixed on the LS holder placed underneath the water surface in the center of the trough, parallel to the moving barriers. The surface film was lowered onto the substrate by removing the subphase water using a water pump at the desired surface pressure.[78] The sharp borders of the LS holder allowed keeping the surface pressure constant to preserve the initial morphology during the transfer.

2.2.2. Atomic force microscopy imaging

After deposition, films were dried in a clean box in the fume hood at room temperature and then scanned by atomic force microscopy (AFM) in tapping mode. A multimode AFM with a Nanoscope V controller (Digital Instruments/Veeco, Santa-Barbara, USA) was used with silicon tips (Bruker USA: model TESPA, rectangular, no aluminum coating on tip and reflective aluminum coating on backside, spring constant 42 N/m, resonance frequency 320 kHz, tip curvature radius 5 nm; or Nanoworld Innovative Technologies, Arrows NCR model, spring constant 42 N/m, oscillation frequency 285 kHz, tip radius less than 10 nm). All images were obtained at a scan rate 0.999 Hz, and a resolution of 512 x 512 pixels. At least 10 different places were scanned for each sample.

Quantitative information was obtained by image analysis using Nanoscope R (III), version 5.12r2 software. Feature heights in topographic images were measured from the top of the dots relative to the flat area between the dots. Dot widths were measured at the half-height of the dot. The average center-to-center distance between the dots was determined by fast Fourier transform (FFT) analysis when possible; otherwise, they were determined by AFM height profiles.

2.2.3. ATR-IR spectroscopy of ultrathin films

Samples were transferred at different surface pressures on a 24 reflections silicon ATR crystal (50 x 20 x 2 mm parallelogram with a 45° face angle). Spectra were recorded by averaging 512 scans with a 4 cm^{-1} resolution on a Tensor 27 FT-IR spectrometer (Bruker Optics) equipped with a liquid nitrogen cooled HgCdTe detector and a vertical ATR accessory. The IR beam was successively polarized parallel (p) and perpendicular (s) with respect to the incident plane with a KRS-5 holographic polarizer (Optometrics). Single beam polarized spectra were first measured on the sample, then the crystal was carefully rinsed several times with HPLC grade chloroform while carefully kept in the sample holder (to avoid spectral distortions due to a change in position between sample and background measurements). The polarized background single beam spectra were finally recorded and used to calculate the sample absorbance spectra.

CHAPTER 3

RESULTS AND DISCUSSION

3.1. PS-P4VP/naphthol and PS-P4VP/naphthoic acid systems and effect of spreading solution concentration

The interest of investigating the PS-P4VP(46%)/naphthol (NOH) and naphthoic acid (NCOOH) systems arises from the PhD work of S. Roland, who studied these systems in the form of thin films deposited by the dip-coating method.[39,48,49] The presence of these two small molecules in the dip-coating solution using THF as solvent led to two different morphology evolutions as a function of dip-coating rate, which was also different from that for PS-P4VP solutions without any small molecule. Using $CHCl_3$ as solvent, a lamellar morphology was obtained for both systems.[39] In this chapter, we study if the presence of NOH or NCOOH has an influence on ultrathin films of a PS-P4VP copolymer with nearly equal PS and P4VP content, deposited by the LB and LS methods. We check the influence of different solution concentrations on the Langmuir isotherms and on the morphology of the transferred films, and compare this with the films obtained for the small molecule-free block copolymer.

3.1.1. Langmuir compression isotherms

Figure 3-1 shows Langmuir isotherms of PS-P4VP (46%) both alone and mixed with NOH and NCOOH (equimolar to VP), all spread from $CHCl_3$ solutions of different concentrations. The first observation is that the isotherms have a similar shape for all systems. For a given system, the isotherms are coincident for all solution concentrations below the plateau region. However, the plateau appears well-defined only at low solution concentrations: at 0.1, 0.5 and 1.0 mg/mL for PS-P4VP and PS-P4VP/NCOOH and at 0.1 and 0.5 mg/mL for PS-P4VP/NOH.

a)

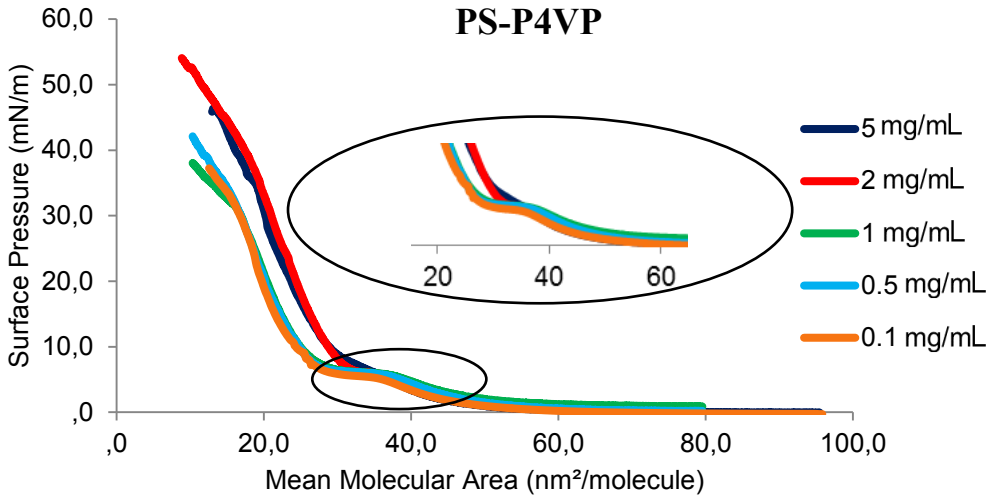

b)

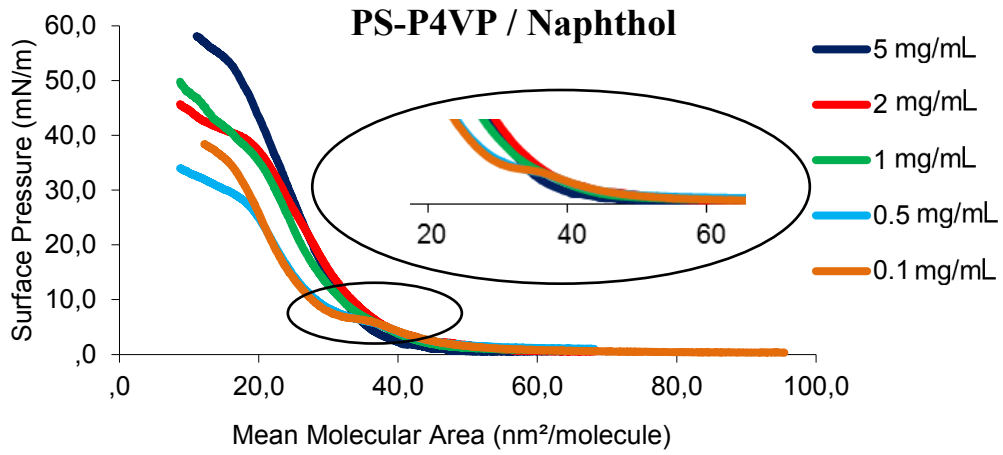

c)

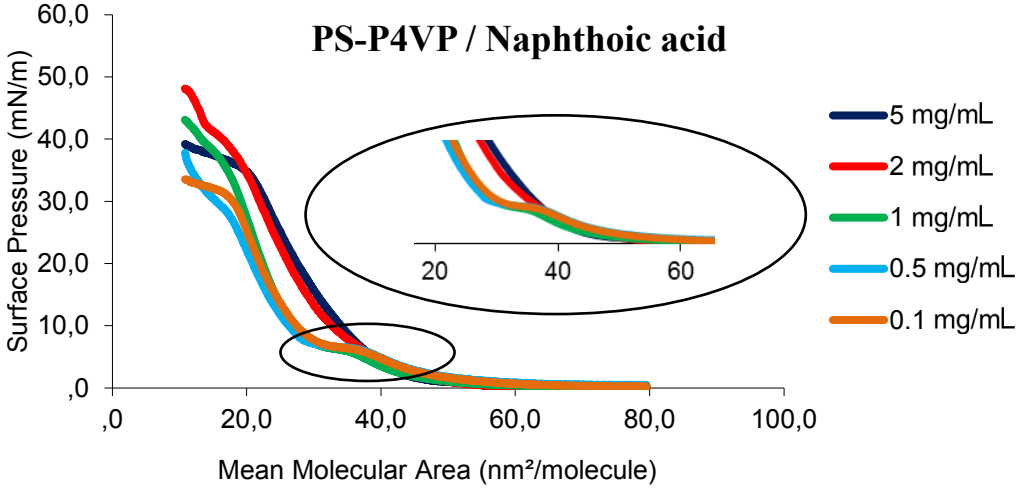

Figure 3-1. Langmuir compression isotherms of (a) PS-P4VP, (b) PS-P4VP/naphthol, (c) PS-P4VP/naphthoic acid spread at 21.0±0.5ºC from $CHCl_3$ solution at the polymer concentrations indicated.

At the higher concentrations, a very short, sloping plateau can be seen for pure PS-P4VP, but the plateau appear monotonic for the small molecule-containing solutions (except on PS-P4VP/NOH at copolymer concentration of 1 mg/mL)

The plateau, when present, is found at a constant surface pressure of about 6 mN/m for both small molecules and in the absence of small molecule. This contrasts with the effect of PDP with PS-P4VP (46%), for which the plateau appears at a much higher surface pressure of 37 mN/m.[71] It was also observed previously, in PS-P4VP systems where P4VP was quaternized with linear alkyl chains of different lengths, that the plateau height increases with increasing alkyl chain length.[79] Clearly, the alkyl chains have an important role. In the case of NOH and NCOOH-containing systems, the constant height of the isotherm plateau, which is the same as for the pure block copolymer, can be related to the short length of the NOH and NCOOH molecules. The small amount that is spread might also solubilize, at least partially, in the water subphase. This is suggested by the isotherm obtained for pure NCOOH (Figure 3-2), which hardly rises above zero surface pressure. The isotherm for the NOH did not change from zero.

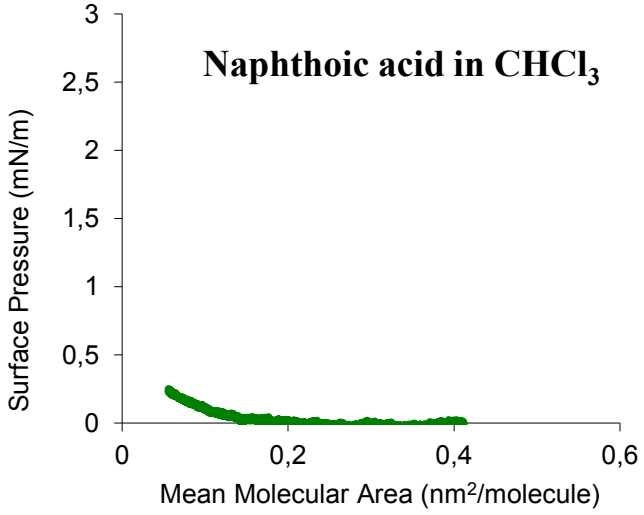

Figure 3-2. Langmuir compression isotherm of naphthoic acid spread from $CHCl_3$ solution (concentration 1.8 mg/mL).

As for the length of the isotherm plateau for low spreading solution concentrations, it is about the same for the systems with and without small molecule present. In previous work, the length of the plateau was found to depend on the hydrophilic block content and is not influenced by the presence of small molecules.[71,79] When the plateau is present (lower concentration solutions), the isotherms rise to higher surface pressures at lower molecular areas than for higher concentration solutions. In general, the isotherm rise above 6 mN/m is approximately parallel for all concentrations until the collapse pressure.

3.1.2. Langmuir - Blodgett and Langmuir - Schaefer monolayer morphologies

LB and LS films of PS-P4VP in pure form and with equimolar NOH and NCOOH present, prepared from five different solution concentrations (5, 2, 1, 0.5, 0.1 mg/mL) and deposited onto mica substrates at two different surface pressures (2 and 10 mN/m), were obtained and their morphologies were imaged by AFM. It was noticed that the transfer ratios of LB films deposited at low surface pressure were generally high (0.9±0.1) for all systems and all solution concentrations. Samples deposited at high surface pressure had more variable transfer ratios ranging from low to high (0.1 to 1).

Table 3-1 shows representative AFM height images of LB films of pure PS-P4VP transferred at surface pressures below (2 mN/m) and above (10 mN/m) the isotherm plateau. Complementary images of LS films are shown for 10 mN/m only, since those for 2 mN/m are not distinguishable from images of the LB films at this pressure. A dot or spherical morphology is evident in all of the images, but their organization changes with changing experimental conditions, as described next.

Table 3-1. AFM height images of LB and LS films of pure PS-P4VP prepared from different solution concentrations and transferred at two different surface pressures (π). The number in the left upper corner indicates the transfer ratio (TR) and "z" refers to the z-scale of the images. The image size is 3 x 3 μm^2 for $\pi = 2$ and 3 x 1.5 μm^2 for $\pi = 10$.

Solution concentration (mg/mL) \ System	PS-P4VP	
π (mN/m)	**π = 2** (z: 5±1 nm)	**π = 10** (z: 5±1 nm)
5	**a)** 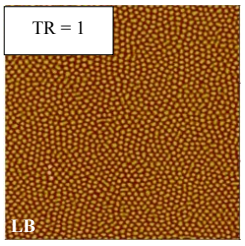	**f)** 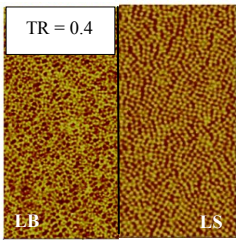
2	**b)** 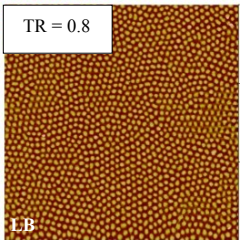	**g)** 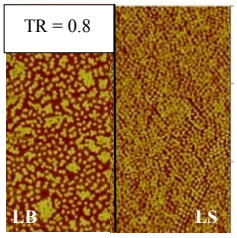
1	**c)** 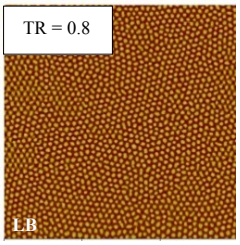	**h)** 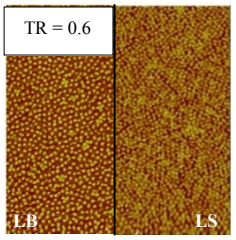
0.5	**d)** 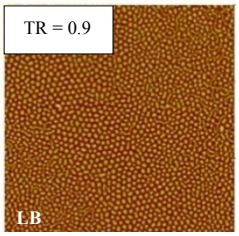	**i)** 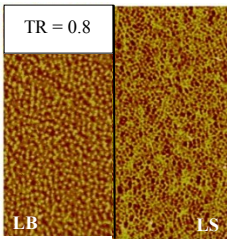
0.1	**e)** 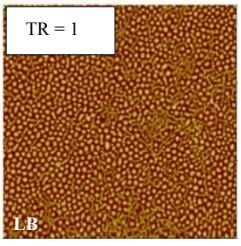	**j)** 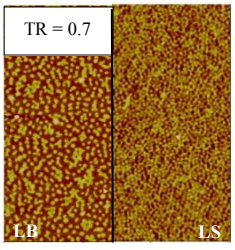

In films transferred at low surface pressure (2 mN/m, below the isotherm plateau), the dots clearly tend to have hexagonal order (by eye) for spreading solution concentrations of 5, 2, and 1 mg/mL (Table 3-1, a-c). For the lower concentration of 0.5 mg/mL, a few elongated structures interspersed among the dots can be observed (Table 3-1d). Elongated structures of lower height than the isolated dots are more visible when the solution concentration is decreased further to 0.1 mg/mL (Table 3-1e). These structures make the hexagonal-like order of the isolated dots less obvious.

For films deposited at high surface pressure (10 mN/m, above the isotherm plateau), differences in morphology and order are observed between LB and LS films. In general, both types of films show significant clustering of dots, contrasting with clear separation of the dots (when excluding the minority elongated structures) in the films deposited at the low surface pressure. For the LS films, there is a clear tendency of the dots to have square-like order [perhaps most clearly evident for the image in Table 3-1f(right) for the 5 mg/mL concentration]. This is evident even when there is significant dot clustering. For the LB films, square-like order is not evident, except somewhat for the 5 mg/mL concentration [Table 3-1f(left)]. We postulate that the high-pressure state imposed at the water surface might relax a little as the film is transferred from the water surface to the substrate (where there is no lateral pressure) and before there is sufficient adherence to the substrate to keep the order intact. This might be exacerbated by the presence of clusters. The appearance of dot clusters in films transferred above the plateau pressure for pure PS-P4VP was mentioned previously by Iryna Perepichka, who also found that the clustering increases with increasing surface pressure (see Figure S1).[80]

In summary, for the pure PS-P4VP solutions, it is clear that, regardless of solution concentration, the dots tend to be hexagonally ordered at low surface pressure, as shown by both LB and LS (not shown) films, whereas they tend to be ordered in a square-like pattern at high surface pressure (as shown by LS films). In addition, at high surface pressure there is a tendency of the dots to aggregate or cluster to some extent. The change from hexagonal-like to square-like order thus

confirms what was observed by our group for the PS-P4VP(46%) and PS-P4VP(29.4%)/PDP systems and that was interpreted as a pressure-induced order-order transition taking place at the plateau pressure.[74] Above the plateau pressure, increasing pressure then simply pushes the dots still closer together, resulting in their clustering, and this clustering tends to increase with increasing pressure.

Table 3-2 shows representative AFM images for the PS-P4VP/NOH system for different spreading solution concentrations. Again, images of only LB films are shown for low surface pressure (2 mN/m), due to the similarity of the LS films, whereas images of both LB and LS films are presented for high surface pressure (10 mN/m). For this system at low surface pressure (π = 2 mN/m), isolated dots are observed only for the three lowest spreading solution concentrations (0.1, 0.5 and 1 mg/mL, Table 3-2c and d), and their order is not very clear, with some local areas appearing square-like, others hexagonal-like and still others with no particular order. For the lowest concentration, there are also elongated, somewhat interconnected structures among the dots. These structures are lower in height than the dots, like for pure PS-P4VP (Table 3-1e). At the highest concentrations (5 mg/mL, Table 3-2a), there is the formation of what can be described as a sponge-like structure of fairly uniform height, as if the dots have coalesced or merged into a kind of network with holes. The same type of structure is present for the concentration of 2 mg/mL (Table 3-2b), except that the height is less uniform and more suggestive of the presence of (partially merged) dots, even with some almost isolated dots.

Table 3-2. AFM height images of LB and LS films of PS-P4VP/NOH prepared from different solution concentrations and transferred at two different surface pressures (π). The number in the left upper corner indicates the transfer ratio (TR). The size of images deposited at π = 2 is 3 x 3 μm^2, at π = 10 is 3 x 1.5 μm^2.

Solution concentration (mg/mL) \ System / π (mN/m)	**PS-P4VP/NOH**	
	π = 2 (z: 4±1 nm)	**π = 10** (z: 4±1 nm)
5	**a)** 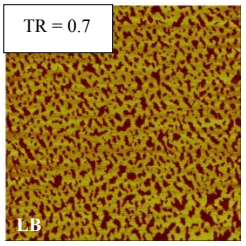	**f)** 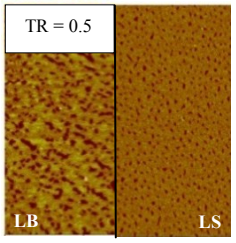
2	**b)** 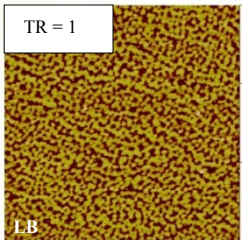	**g)** 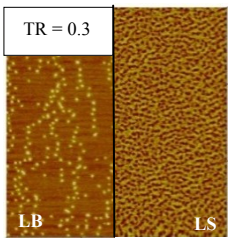
1	**c)** 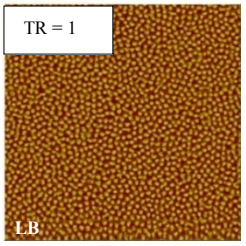	**h)** 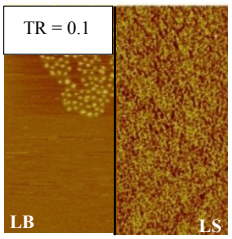
0.5	**d)** 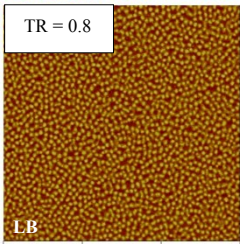	**i)** 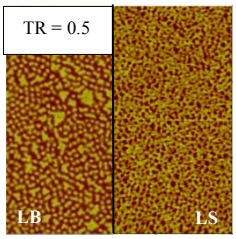
0.1	**e)** 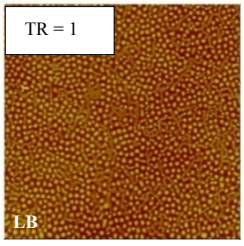	**j)** 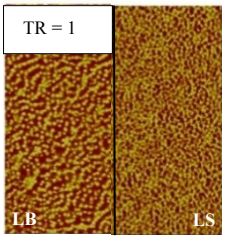

For high surface pressure (10 mN/m), the image of the LS film obtained from the most concentrated solution (5 mg/mL; Table 3-2f) shows the same sponge-like structure as at low surface pressure, but it is more condensed and thus has fewer and smaller pores. A similar morphology is observed in the LB film, but less condensed, again suggesting that some relaxation or deformation of the high pressure state occurs during the LB transfer to the substrate. Such relaxation may be greater when the transfer ratio is lower (here, 0.5). The LS film obtained from the solution concentration of 2 mg/mL also shows the sponge-like structure similar to the low pressure film (Table 3-2g). The corresponding LB film shows only isolated, scattered dots or short chains of dots, probably due to the very low transfer ratio (0.3), and thus is not representative of the morphology on the water surface. The absence of isolated dots and the similarity of the low- and high-pressure morphologies for these two concentrations can explain the absence of a plateau in the Langmuir isotherms for these two concentrations. For the three lower solution concentrations, the LS films transferred at high pressure show a different morphology from that of the films transferred at low pressure. This is consistent with the presence of a plateau in the Langmuir isotherms for 0.1 and 0.5 mg/mL, but not with the absence of a plateau for 1.0 mg/mL. The morphology observed appears to be based on a square-like order of dots, although the squares tend to show connections between their corners suggesting some merging of the dots along the square edges and with neighbouring squares. The corresponding LB films show more isolated dots as well as dot clusters without any particular order, but they are less likely to be representative than the LS films because of the low transfer ratios (especially for 1 mg/mL, Table 3-2h, for which the transfer ratio is 0.1) and/or possible relaxation of the lateral stress during transfer, as mentioned above.

In Table 3-3, the analogous series of AFM height images for the PS-P4VP/NCOOH system is presented, again with LB films only at low surface pressure and LB and LS films at high surface pressure for the same reason as stated above. The trends for PS-P4VP/NCOOH are somewhat similar to those just described for PS-P4VP/NOH.

Table 3-3. AFM height images of LB and LS films of PS-P4VP/NCOOH prepared from different solution concentrations and transferred at two different surface pressures (π). The number in the left upper corner indicates the transfer ratio (TR). The size of images deposited at π = 2 is 3 x 3 μm^2, at π = 10 is 3 x 1.5 μm^2.

Solution concentration (mg/mL) \ System / π (mN/m)	**PS-P4VP/NCOOH**	
	π = 2 (z: 3±1 nm)	**π = 10** (z: 3±1 nm)
5	**a)** 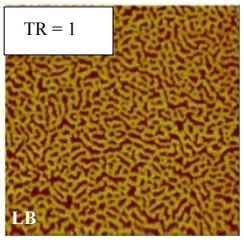	**f)** 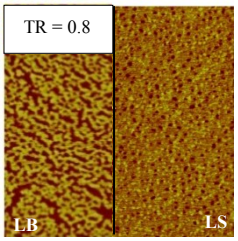
2	**b)** 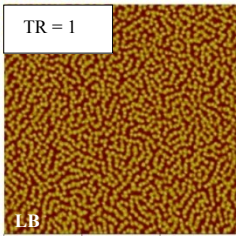	**g)** 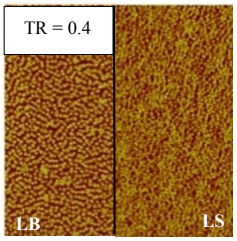
1	**c)** 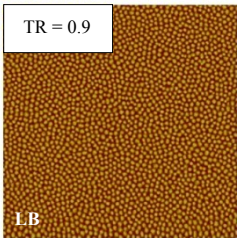	**h)** 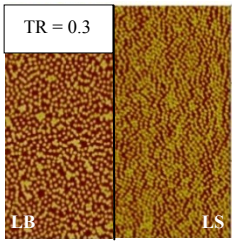
0.5	**d)** 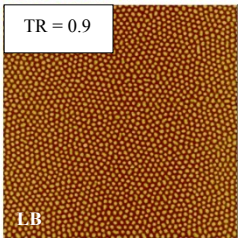	**i)** 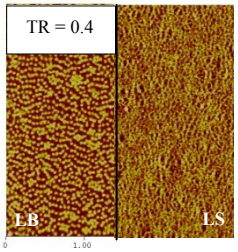
0.1	**e)** 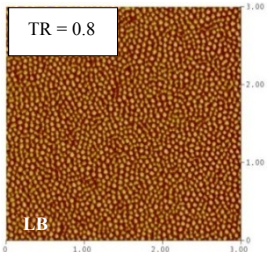	**j)** 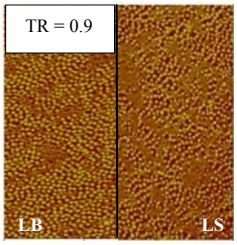

At low surface pressure (2 mN/m), the two highest concentration solutions show a similar morphology that can be described as a kind of interconnected worm-like network (sponge-like but better defined), except that for 2 mg/mL (Table 3-3b), the dots comprising the network are clearly distinguishable (in the form of interconnected linear sequences), whereas for 5 mg/mL(Table 3-3a) they appear to have fused completely. For the three lowest solution concentrations (Table 3-3c, b and e), there are again individual dots that tend to be ordered hexagonally (most clearly for 0.5 mg/mL). For the most dilute solution (0.1 mg/mL), there is also a tendency for some dots to form more closely spaced linear sequences, as if tending towards the elongated structures observed for low concentration solutions of PS-P4VP and PS-P4VP/NOH described above.

For films transferred at high surface pressure (10 mN/m), the images of all of the LS films is consistent with square-like order of the dots (particularly evident for the 1.0 mg/mL concentration), and include dot clusters, with the dots more distinguishable in some cases and more fused in others. For the highest concentration, for which the dots are not distinguishable, the morphology resembles that of the low-pressure film except for being more compressed and appearing to include a higher layer of scattered dots. The image of the LB film for this concentration and also the image for 2 mg/mL (but with some dot clusters for the latter) resemble the corresponding low-pressure images. The LB film images for 1 and 0.5 mg/mL (like for 2 mg/mL) concentration solutions show a mix of disordered dots and dot clusters, the more spaced isolated dots probably again reflection some relaxation of the lateral stress during transfer. The lowest concentration solution (0.1 mg/mL; Table 3-3j) shows what appear to be fused dots of uniformly lower height (reminiscent of the elongated structures of lower height in PS-P4VP and PS-P4VP/NOH films prepared from low concentration solutions, but transferred at low pressure not at high pressure like here). It is of interest to note also that the image of the LB film for this concentration, for which the transfer ratio is high, is quite similar this time to the image of the corresponding LS film. Like for PS-P4VP/NOH, the absence of dots in the low-pressure films prepared from the two highest concentration solutions can explain the absence of a plateau in the

Langmuir isotherms for these concentrations. For the lower concentrations, the presence of the isolated dots and change in their order between low and higher surface pressure is consistent with the presence of this plateau in the isotherms for those concentrations.

The morphologies of the three different systems for the different spreading solution concentrations and at low and high surface pressures are summarized in Table 3-4.

Table 3-4. Solution concentration and surface pressure dependence on the LB and LS films morphologies for the following systems.

System / Solution concentration (mg/mL) \ π (mN/m)	**PS-P4VP**		**PS-P4VP/NOH**		**PS-P4VP/NCOOH**	
	π=2	**π=10**	**π=2**	**π=10**	**π=2**	**π=10**
5	**d_{hex}**	**d_{sq}**	**s**	**s**	**s**	**s**
2	**d_{hex}**	**d_{sq}, da**	**s, d**	**s, d**	**s, d**	**s, d_{sq}, da**
1	**d_{hex}**	**d_{sq}**	**d**	**d**	**d_{hex}**	**d_{sq}**
0.5	**d, e**	**d_{sq}, e**	**d**	**d, da**	**d_{hex}**	**d_{sq}**
0.1	**d, e**	**d_{sq}, da**	**d, e**	**d, e**	**d, e**	**d, e**

d - dots, s - sponge, e - elongated structures, da – dot aggregates

At low surface pressure, most of the LB (and LS) films prepared from the solutions of the pure diblock copolymer have a pure or majority isolated dot structure tending to hexagonal order. In contrast, the presence of small molecules in system (NOH, NCOOH) gives rise to the appearance of a sponge-like or network-like morphology for the most highly concentrated solutions and isolated dot structures for less concentrated solutions. Thus, for the latter (1-0.1 mg/mL concentrations), the morphology of the LB films of the pure block copolymer and those containing small molecules are similar. They also tend to include a minor component composed of elongated structures that are generally lower in height than the dots for the lowest solution concentrations, best observed for 0.1 mg/mL solutions of PS-P4VP and PS-P4VP/NOH.

At high surface pressure, the film structures are best observed in LS films, where the dot structures tend to organize in a square-like structure. This is perfectly clear for the pure diblock copolymer and less expressed for PS-P4VP/NCOOH and PS-P4VP/NOH. For the latter two systems at the highest concentrations (2 and 5 mg/mL), since the dots are fused (i.e. absent) or aggregated in a network-like structure at low pressure, they are also absent or highly aggregated at high pressure, thus rationalizing the absence of a plateau in the corresponding Langmuir isotherms. The LB films obtained at high pressure probably reflect some relaxation of lateral stress during the transfer process, especially pronounced for low transfer ratios, and thus tend to show somewhat looser structures than the LS films, such as less organized and more separated isolated dots as well as dot clusters.

The less defined morphology of the PS-P4VP/NOH and PS-P4VP/NCOOH films, especially for the higher solution concentrations, can be the result of partial compatibility of NOH and, to a lesser extent, NCOOH with the PS phase, as was found earlier by DSC measurements.[39] This might reduce the segregation strength between PS and P4VP, which can have the effect of reducing well defined phase separation. If this is true, it also indicates that the small molecules must be present as the films develop their morphology on the water surface, and not dissolved (or at least not fully dissolved) in the water subphase. In future work, it will be of interest to try to verify this by infrared techniques, as used in the next chapter and as indicated in the final chapter.

3.1.3. Dimensions of nanofeatures

The dimensions of the nanofeatures – particularly the heights, diameters and center-to-center distances of nearest features – in the LB and LS films is of interest to compare for the different systems under the different experimental conditions. For example, in our previous work as described in Chapter 1, this analysis helped in the interpretation of the isotherm plateau as an order-order transition. All geometrical parameters were measured using the AFM software program. At least ten different places of each sample were scanned, at least three reproducible images

of different sizes were obtained. For the center-to-center distances, a two-dimensional FFT (fast Fourier transform) function was applicable to the images with size of 3 μm (unless otherwise indicated), which was only possible for the morphologies composed of isolated dots. The center-to-center distances of the dots mixed with other structures was measured manually from the 1 μm images.

The nanofeature dimensions of PS-P4VP, PS-P4VP/NOH, PS-P4VP/NCOOH LB films deposited at low surface pressure (2 mN/m) are summarized in Table 3-5. It should be noted that measuring the widths and center-to-center distances is not possible for the sponge-like structures observed for LB films of small molecule-containing systems prepared from high concentration solutions. Clearly, most of the geometrical parameters involving the isolated dot morphologies are similar for all three systems within experimental uncertainty: the heights are 2.6±0.3 nm, the widths are 40±5 nm, and the center-to-center distances are usually 65±5 nm. The center-to-center distances tend to be somewhat lower in the PS-P4VP/NCOOH films, which might be related to some square-like order in these films already for low surface pressures (it is also of interest to note that the distance measured for the 1 mg/mL film is the same, at 55 nm, as the distance between dots that form part of the nascent network in the 2 mg/mL film). In contrast, the low-concentration elongated structures dispersed among the dots and the high-concentration sponge-like structures are noticeably lower in height at about 1.3±0.1 nm in most cases (thus about half the height of the isolated dots), as if merging of the PS phase into more interconnected structures reduces their repulsion from the aqueous surface. It is notable that the intermediate situation for the NCOOH system at 2 mg/mL, where the dots tend to form a network but are still highly distinguishable, also shows an intermediate height value.

Table 3-5. Heights (*h*), widths (*w*) and center-to-center distances (*d*) of the nanofeatures in LB films of PS-P4VP, PS-P4VP/NOH, PS-P4VP/NCOOH spread from different spreading solution concentrations and transferred at π = 2 mN/m.

System / Solution concentration (mg/mL)	PS-P4VP			PS-P4VP/NOH			PS-P4VP/NCOOH		
	h (nm ±0.5)	*w* (nm ±5)	*d* (nm ±10)	*h* (nm ±0.5)	*w* (nm ±5)	*d* (nm ±10)	*h* (nm ±0.5)	*w* (nm ±5)	*d* (nm ±10)
5	2.4	35	75	1.3	n/a	n/a	1.4	55	n/a
2	2.6	38	70	1.2	n/a	n/a	2.0	45	55* 75•
1	2.5	43	67	2.5	45	70	2.2	49	55
0.5	2.5	40	63	2.3	42	64 55*	2.4	34	60
0.1	2.5(d) 0.7(e)	40(d) 35(e)	64 (d)	2.2(d) 1.3(e)	50(d) 35(e)	65(d)	2.9(d) 1.1(e)	30	64[m]

* in row, • between the rows, [m] measured manually by AFM height profiles
(d) applicable for dots, (e) applicable for elongated structures

Nanofeature dimensions for PS-P4VP, PS-P4VP/NOH, PS-P4VP/NCOOH LB and LS films deposited at the surface pressure of 10 mN/m are reported in Table 3-6. In general, the heights and widths of the nanofeatures in the high-pressure films are similar to those in the low-pressure films (within experimental uncertainty) and also tend to be similar for films deposited by the LB and LS methods. It was of particular interest to try to find any changes in the height of the background, as was described for the PS-P4VP/PDP system.[74] However, no evidence of increasing background height could be found, as reported previously for the pure PS-P4VP system, and, at the same time, the height of dots is constant below and above the isotherm plateau pressure for the small molecule-containing systems (like for the pure PS-P4VP system). The only geometrical parameter that

changes significantly is center-to-center distance (when measurable), which is generally significantly lower in the high-pressure films compared to the low-pressure films, as expected due to the compression at the air/water interface. This was most clearly measured for the PS-P4VP system. In the case of sponge morphologies, this measurement was not possible, and in other cases, the dots were too close or too unclear to allow this measurement.

Table 3-6. Heights, widths and center-to-center distances of the nanofeatures in LB and LS films of PS-P4VP, PS-P4VP/NOH, PS-P4VP/NCOOH spread from different solution concentrations and transferred at π = 10 mN/m.

System / Solution concentration (mg/mL)	PS-P4VP			PS-P4VP/NOH			PS-P4VP/NCOOH		
	h (nm ±0.5)	*w* (nm ±5)	*d* (nm ±10)	*h* (nm ±0.5)	*w* (nm ±5)	*d* (nm ±10)	*h* (nm ±0.5)	*w* (nm ±5)	*d* (nm ±10)
5	2.9 2.7^{LS}	44 46^{LS}	n/a 65^{LS}	1.4	n/a	n/a	1.6 $0.8^{LS\,\#}$	n/a	n/a
2	2.8 2.8^{LS}	41 41^{LS}	n/a 55^{LS}	2 1^{*}	40 n/a^{LS}	n/a	2.3 $2.2^{LS\,\#}$	39 40^{LS}	67^{*m},$85^{\bullet m}$ n/a^{LS}
1	2.2 2.4^{LS}	36 37^{LS}	65 63^{LS}	1.8 2.3^{*}	37 $n/a^{*\,LS}$	n/a	2.4 2.4^{LS}	35 39^{LS}	65 $61^{LS\,*\,m}$
0.5	2.5 2.7^{LS}	40 40^{LS}	60 53^{LS}	2.4 2.2^{*}	50 48^{LS}	65	2.2 2.4^{LS}	33 36^{LS}	64 n/a
0.1	2.5 2.7^{LS}	38 39^{LS}	n/a 54^{LS}	2.5 2.6^{*}	53 50^{LS}	n/a	2.7 2.8^{LS}	35 37^{LS}	65^{*m} $92^{\bullet m}$

* in row, $^{\bullet}$ between the rows, ^{m} measured manually

^{LS} indicates values for the LS films

$^{\#}$ the height of structure was measured relative to the lowest parts of morphology

3.1.4. Conclusions

Using a PS-P4VP(46%) block copolymer and its hydrogen-bonded complexes with NOH and NCOOH, spread at the air/water interface from $CHCl_3$ solutions of five different concentrations and deposited by the LB and LS techniques at two surface pressures (below and above the isotherm plateau), we reached the following conclusions. The shape of the Langmuir isotherms is similar for all systems, where the presence or absence of an isotherm plateau depends on the spreading solution concentration. In particular, it is absent for high solution concentrations except for pure PS-P4VP, which gives a short, diagonally oriented plateau. When present, it appears at 6 mN/m for all three systems. The same position of the isotherm plateau for the small molecule-containing systems and for the pure block copolymer can be explained by the relatively small size of these small molecules that do not contain alkyl chains and also by possible partial solubilisation in the water subphase.

Examination of the LB and LS film morphologies by AFM indicate that, for PS-P4VP, the order-order transition from hexagonal-like to square-like can be observed regardless of the solution concentration. The square-like order is most clearly observed in LS films, probably due to some relaxation of the lateral stress occurring during LB transfer at the higher surface pressure, or to deformation of the film organization caused by shear or capillary forces, exacerbated by the generally lower transfer ratios. It was found previously by our group that the pressure-induced order-order transition is clearly observed for the PS-P4VP(29.4%)/PDP system as well as for the pure block copolymer, investigated only for the solution concentration of 1.8 mg/mL.[74] In the current study, we have shown, in addition, that some elongated structures of lower height than the dots are interspersed as a minority component among the dots in the low-pressure films prepared from the lowest concentration solutions.

In the presence of NOH and NCOOH, the same order-order transition is apparent only when the spreading solution concentration is not too high (about 1 mg/mL or less). For concentrations of 2 and 5 mg/mL, the low-pressure

morphology is sponge-like or network-like; i.e. there is no well-dispersed dot morphology. In these cases, the high-pressure morphology is similar to the low-pressure one, just more compressed. This also explains the absence of a plateau in the Langmuir isotherms in these cases. The sponge-like and network-like structures (which, like the elongated structures for low-concentration solutions, are lower in height than the isolated dots) may be related to some compatibility of NOH and, to a lesser extent, NCOOH with the PS phase, which could reduce the extent of phase separation. As for the dimensions of the nanofeatures, there is little difference between the films of all three systems at low surface pressure. At high surface pressure, the nanostructures tend to be closer together, as a result of lateral compression.

3.2. PS-P4VP/PDP system. From macroscopic 2D order-order transition to molecular level reorganization

As indicated in the introduction, LB and LS monolayer films of amphiphilic diblock copolymers giving a dot morphology show a first-order transition in the Langmuir isotherm and it was found previously that this transition corresponds to an order-order transition of the dots between hexagonal and square.[71,74] Here, we confirm these results for PS-P4VP with and without PDP present, and then we undertake an IR analysis of the PS-P4VP/PDP system to try to detect what molecular changes accompany this macroscopic order-order transition.

3.2.1. Confirmation of order-order transition

Previously published results[74] were reproduced here and are summarized in Figure 3-3 for our block copolymer with similar molecular weight (PS-P4VP(30.3%)). The Langmuir isotherms of PS-P4VP(46%) and PS-P4VP(30.3%)/PDP (1:1 VP:PDP), spread from chloroform solutions at the air/water interface, show the expected plateau associated with the first-order transition at surface pressures of 6 and 36 mN/m, respectively. The AFM images of monolayer films transferred to mica show that the 2D organisation of the dots changes from hexagonal-like below the plateau to square-like above the plateau in accordance with our previous studies.[71,74]

As a reminder, the dots are composed of the PS block, which is hydrophobic and assembles into micelle-like aggregates to avoid the water surface as much as possible, while the surrounding matrix is composed of hydrophilic P4VP spread as a monolayer on the water surface (including beneath the PS aggregates). The PDP, when present, is associated with the P4VP monolayer due to the ability of its phenol head group to hydrogen bond to P4VP and/or to the water surface, while the alkyl chains, which are hydrophobic, must lie above the P4VP/phenol layer, which, at the same time, reduces the interfacial energy with air.

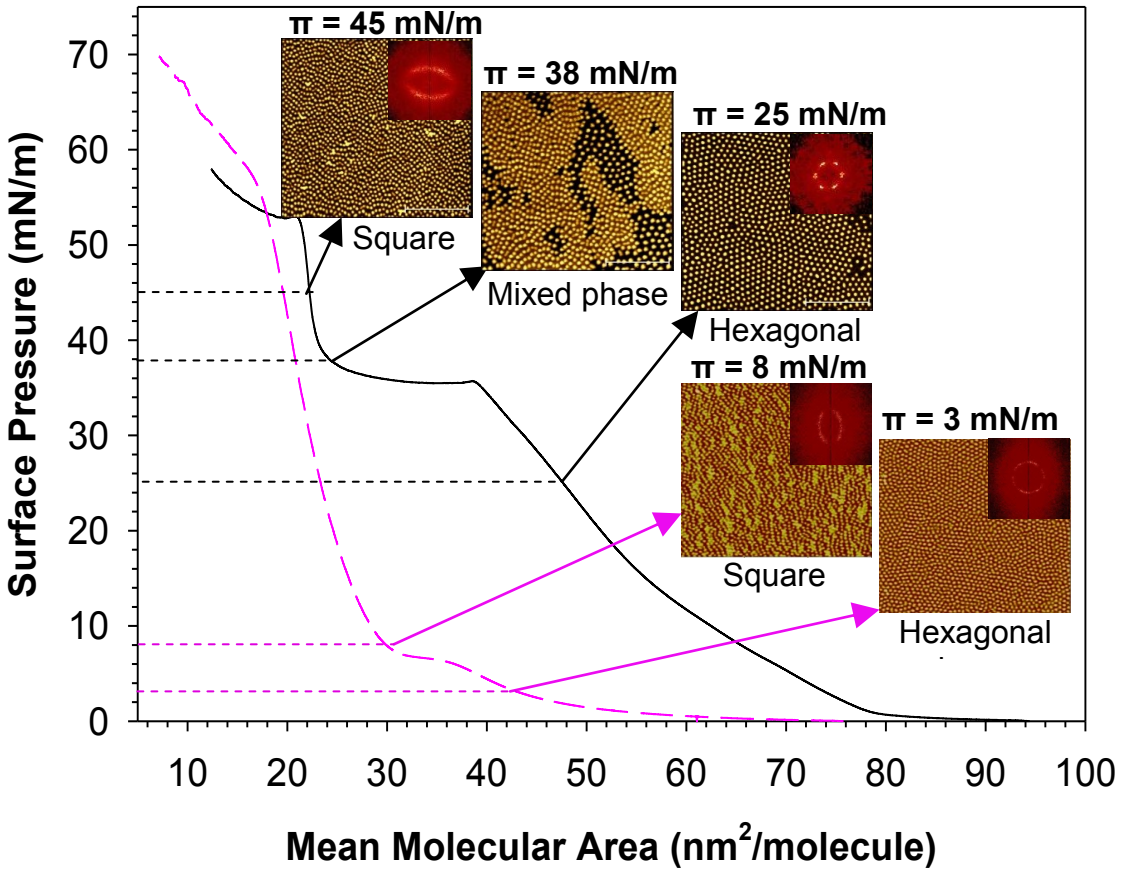

Figure 3-3. Langmuir compression isotherms of PS-P4VP(30.3%)/PDP (black curve) and PS-P4VP(46%) (pink curve) at the air/water interface. AFM height images (3x3 μm^2) of Langmuir-Blodgett monolayer films transferred onto mica at the surface pressures indicated.

The reason for choosing a copolymer with a higher P4VP content for the PDP-free system is that the pure PS-P4VP(30.3%) block copolymer gives rise to a nanostrand morphology mixed with the dot morphology (see Figure S2), and therefore cannot be compared directly with the dot morphology of its complexed homologue. The much higher surface pressure of the plateau (and its greater length) for the PDP-containing system compared to the PDP-free one is most likely related to the presence of the PDP alkyl chains, which somehow stabilize the lower-pressure phase. This is suggested by investigations of PS-P4VP derivatives with

P4VP quaternized by alkyl chains of varying lengths, where it was found that increasing the alkyl chain length increases both the surface pressure and the length of the plateau.[69,75,81-83]

The AFM image of the PDP-containing film transferred at a surface pressure close to the plateau value shows the coexistence of the two phases, with the matrix increasing in thickness by 2.4 ± 0.2 nm at the transition. The width of the dots is reduced from 55±5 nm to 46±4 nm when increasing the surface pressure from 25 to 45 mN/m, which can be explained by the thicker matrix hiding the lower part of the dots. In contrast, no significant differences in matrix thickness, dot height or dot width was detectable for the pure block copolymer, probably because, without PDP present, the difference is smaller than what is detectable by AFM (i.e. smaller than a few Å).

It must be emphasized that a first-order transition (plateau) in the LB isotherm is well established for dot-forming amphiphilic block copolymers where the hydrophilic block is associated either covalently or by hydrogen bonding with long alkyl chains.[74] For a time, it was more controversial for amphiphilic block copolymers without lengthy alkyl chains, but has now been reported for various PS block copolymers, including PS-poly(methyl methacrylate) (PS-PMMA),[84] PS-poly(ethylene oxide) (PS-PEO),[76] PS-poly(n-butyl methacrylate),[70] PS-poly(t-butyl methacrylate),[70] and PS-poly(acrylic acid).[85] The discovery that the plateau is associated with an order-order transition is more recent;[74] however, examination of some images provided in the literature gives evidence of the transition – for example, for PS-PMMA[85], PS-PEO[86], and alkylated (decylated) PS-P4VP[75]

3.2.2. Infrared investigation of molecular-level changes

In earlier efforts to understand the isotherm plateau, various researchers investigated molecular-level changes. For example, conformational changes of the P4VP chains at the air/water interface (such as reorientation of the pyridine rings from flat to edge-on relative to the water surface) may occur.[75] For alkylated PS-P4VP, infrared spectroscopy investigations at the air/water interface indicated

alkyl chain ordering.[76] This was taken as suggestive of an alkyl chain reorientation at the plateau from prone to more vertical relative to the air/water interface that accompanies the order-order transition and that can rationalize the increase in matrix thickness of the PDP-containing system.[74] Here, our objective is to deepen the understanding of the molecular changes that accompany the macroscopic order-order transition by conducting an infrared spectroscopic analysis of monolayer films transferred at surface pressures below and above the isotherm plateau.

First, conformational changes of the PDP alkyl chains will be investigated. The conformation can be probed by the band positions of the CH_2 elongation modes in the IR spectra. Figure 3-4 presents the spectra of PS-P4VP(30.3%)/PDP transferred at surface pressures of 25 and 45 mN/m, measured with "p" polarization.

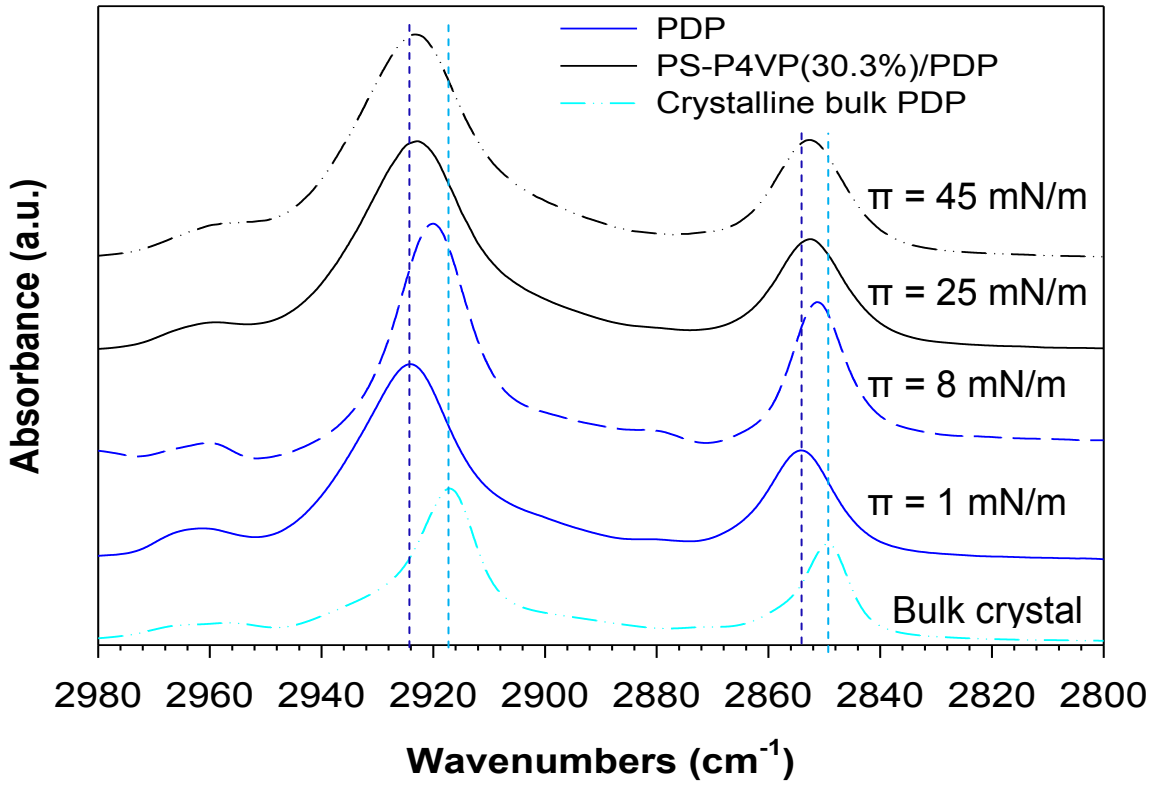

Figure 3-4. IR spectra in p-polarization for LB films of PDP and PS-P4VP(30.3%)/PDP transferred onto a silicon crystal at the surface pressures (π) indicated, in comparison to the bulk spectrum of PDP in the crystalline state.

The bands centered around 2923 and 2852 cm^{-1} are due to the anti-symmetric and symmetric CH_2 elongations, respectively.[87] The position of these bands is known to shift to lower wavenumbers when the CH_2 groups adopt a trans conformation, such as in the crystalline state, and to higher wavenumbers when they adopt more gauche conformations such as in the liquid state. This spectral region is dominated by PDP due to the numerous CH_2 groups of the PDP alkyl chains as compared to PS and P4VP. For comparison, the spectra of the bulk crystalline form of PDP and of pure PDP monolayers transferred before and after a plateau situated at a surface pressure of ~6 mN/m are also shown. The plateau value, in this case, is associated with a liquid to liquid crystalline transition of the PDP molecules, as indicated by a band shift to higher wavenumbers from 2925 to 2920 cm^{-1} for the anti-symmetric elongation mode for samples transferred at 1 and 8 mN/m, respectively. This shift is associated with a transition from the significant dominance of *gauche* conformations of the alkyl chains in the liquid state to a greater extent of *trans* conformation, related to the higher level of order of the alkyl chains, in the liquid crystalline state.[88] When the alkyl chains are highly ordered, as in the bulk crystal, the *trans* conformation dominates, giving a band position ~2917 cm^{-1}. Similar shifts are observed for the symmetric elongation mode, as summarised in Table 3-7.

Table 3-7. The precise CH_2 band positions of different samples.

sample	**Bulk crystal**	**PDP**		**PS-P4VP/PDP**	
π (mN/m)		**π = 1**	**π = 8**	**π = 25**	**π = 45**
band position	2917.1	2924.6	2920.1	2922.9	2922.9
	2849.4	2854.2	2851.1	2852.5	2852.6

The position of these bands in the PS-P4VP(30.3%)/PDP system is identical for LB films transferred at both surface pressures, below and above the plateau, and is intermediate to the positions found for the liquid and liquid crystalline states of PDP (close to the liquid state for the asymmetric stretching band and closer to the liquid crystalline state for the symmetric stretching band). These results indicate that the alkyl chains of the PDP molecules in the complex have mainly disordered *gauche* conformations and that no conformational changes are associated with the macroscopic order-order transition observed in the isotherm of Figure 3-3. This conclusion is in disagreement with the in situ IR study of Shin *et al.*[76] on alkylated PS-P4VP monolayers at the air/water interface. They showed that the alkyl chain order increases as a function of the surface pressure and that the effect is amplified by increasing the alkyl chain length. Several reasons could account for the difference with our result. One is that the alkyl chains may relax to a lower energy state toward more disorder during the transfer from the air/water interface to the solid substrate. Another may be the difference in alkyl chain length (C_{15} for us vs. C_{18} for Shin *et al.* and the H-bonded (us) vs. covalently-bonded (Shin *et al.*), along with the ionic character of the pyridinium moieties for the latter; these molecular differences may hinder relaxation from the liquid crystalline (and eventually crystalline) state for the system of Shin *et al*. Overall, the absence of band position changes upon surface pressure increase in our case shows that changes in alkyl chain conformation is not a driving force giving rise to the macroscopic 2D order-order transition.

The absence of conformational changes does not exclude the possibility of a change in orientation of the alkyl chains and/or other molecular groups. To address this, polarized ATR spectra were used to quantify orientation. Figure 3-5 presents two spectral regions of the polarized ATR spectra of PS-P4VP(30.3%)/PDP monolayers transferred onto silicon substrates at surface pressures of 25 and 45 mN/m.

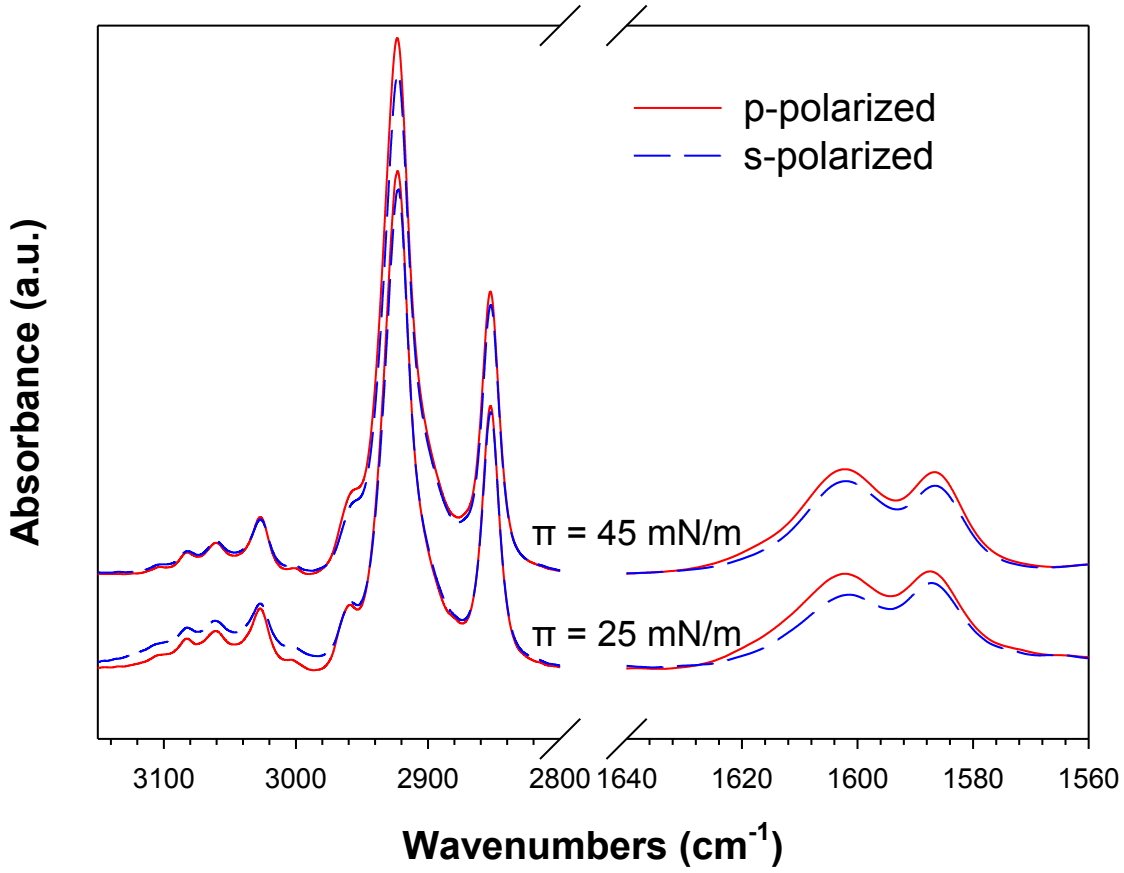

Figure 3-5. Polarized ATR spectra of Langmuir-Blodgett PS-P4VP(30.3%)/PDP films transferred to a silicon crystal at surface pressures of 25 and 45 mN/m (below and above the isotherm plateau value).

The differences in signal intensity for the "p" and "s" polarizations depends on the in-plane versus out-of-plane orientation of the molecules with respect to the substrate. To evaluate orientation, one must quantify the $\langle P_2 \rangle$ value, which is 0 for a totally isotropic distribution and 1 for perfect out-of-plane orientation of the units. As described in section 1.4.2, the absorbance of the sample is related to mean square electric field amplitudes of the evanescent polarized radiation in the film. This effect modifies the relative intensities of the polarized spectra and must be taken into account in the quantification of $\langle P_2 \rangle$. The very high signal-to-noise ratio

of the spectra presented Figure 3-5 allows using these absorbance differences to evaluate molecular orientation.

Table 3-8 summarises the $<P_2>$ values quantified for the main bands in the spectra of Figure 3-5. The results were averaged over 3 independent samples prepared in the same conditions. The standard deviation is very low for all of the bands investigated, highlighting the good reproducibility of the results. The values for the CH_2 stretching modes were quantified taking into account a tilt angle of the transition dipole moment of 90° with respect to the alkyl chain of PDP.[87] The values range from 0.28 to 0.37 and indicate a relatively high overall orientation of the alkyl chains perpendicular to the surface plane. It is noteworthy that no significant changes are observed when comparing $<P_2>$ values for films transferred below and above the isotherm plateau. The orientation of the phenol group of the PDP molecule, measured from the polarized absorbance of the 1587 cm^{-1} band (associated with the C=C stretching of the PDP aromatic ring), shows an isotropic distribution, and it also does not evolve with the transfer surface pressure. However, in this case, orientation cannot be excluded since the rotational flexibility of the phenol OH group with respect to the aromatic ring does not allow its detection.

Table 3-8. $<P_2>$ values for the designated bands, quantified from polarized ATR spectra of PS-P4VP(30.3%)/PDP LB films (n = 3) transferred onto a silicon substrate at the surface pressures indicated.

band position / π (mN/m)	**C-H PS aromatic ring 3060 cm^{-1}**	**CH_2 2923 cm^{-1}**	**PDP 2853 cm^{-1}**	**P4VP and PS aromatic ring 1601 cm^{-1}**	**PDP aromatic ring 1586 cm^{-1}**
π = 25	0.02 ± 0.01	0.32 ± 0.04	0.37 ± 0.05	0.21 ± 0.03	0.01 ± 0.01
π = 45	0.00 ± 0.02	0.28 ± 0.06	0.34 ± 0.06	0.02 ± 0.03	0.02 ± 0.01

Table 3-8 also shows the orientation values of bands associated with the PS-P4VP block copolymer. The 3060 cm^{-1} band is due to C-H stretching of the PS benzene ring.[89] Figure S3 demonstrates that the 3060 cm^{-1} band is dominated by PS, even if P4VP also absorbs in this spectral range. The $\langle P_2 \rangle$ value close to 0 determined for this band is again associated with an isotropic distribution, indicating that the PS aromatic rings (and most likely the PS chains) in the dots are distributed isotropically with respect to the surface normal.

The only significant difference observed between films transferred below and above the isotherm plateau is related to the orientation of the pyridine ring, determined using the 1600 cm^{-1} band due to a ring stretching mode.[90] This mode is parallel to the pyridine C1-N axis, based on DFT calculations, and thus perpendicular to the main chain.[91] Below the plateau, the pyridine ring shows an orientation along the surface normal that is slightly lower than that observed for the PDP alkyl chain, with an average $<P_2>$ value of 0.21. One must, however, consider that a similar stretching mode for the PS benzene ring participates in the overall intensity of this band (see Figure S3) and that P4VP is the minor constituent in PS-P4VP(30.3%). Their relative contributions to the measured absorbance rely on their relative absorption coefficients, which is difficult to evaluate, especially in the context of pyridine complexation with PDP. Accordingly, knowing that PS is isotropic, the $\langle P_2 \rangle$ value associated with the pyridine ring must be higher than the quantified value. This out-of-plane orientation of the pyridine rings contradicts the hypothesis of Kawaguchi *et al.*, who postulated that they should lie flat on the air/water interface for a similar system.[83] Interestingly, when increasing the surface pressure to 45 mN/m, the orientation disappears and the distribution becomes totally isotropic. The physical explanation for this unexpected result will be treated later.

It should be mentioned that the width of the orientation distribution is inversely proportional to the $<P_2>$ value. Quantifying a tilt angle, θ, at which all units would be perfectly aligned, is a common approximation in surface science. However, it is an entropically extremely unlikely scenario for non-crystalline

systems as compared to a smooth Gaussian distribution of the units centered at 0° with respect to the substrate normal but with a broad distribution of θ angles.[92-93]

The investigation of the degree of complexation between P4VP and PDP as well as changes with surface pressure can provide further insight into possible molecular reorganisation occurring at the isotherm plateau. This aspect can be probed by examining the C=C elongation bands of the aromatic rings of P4VP (1600 cm^{-1}) and PDP (1587 cm^{-1}) whose positions are both sensitive to hydrogen bonding.

Figure 3-6 shows the p-polarized spectra of pure block copolymer (PS-P4VP(46%)) monolayers transferred onto a silicon substrate at surface pressures of 3 and 8 mN/m, in comparison to the complex transferred at surface pressures of 25 and 45 mN/m and to pure PDP transferred at surface pressures of 1 and 8 mN/m.

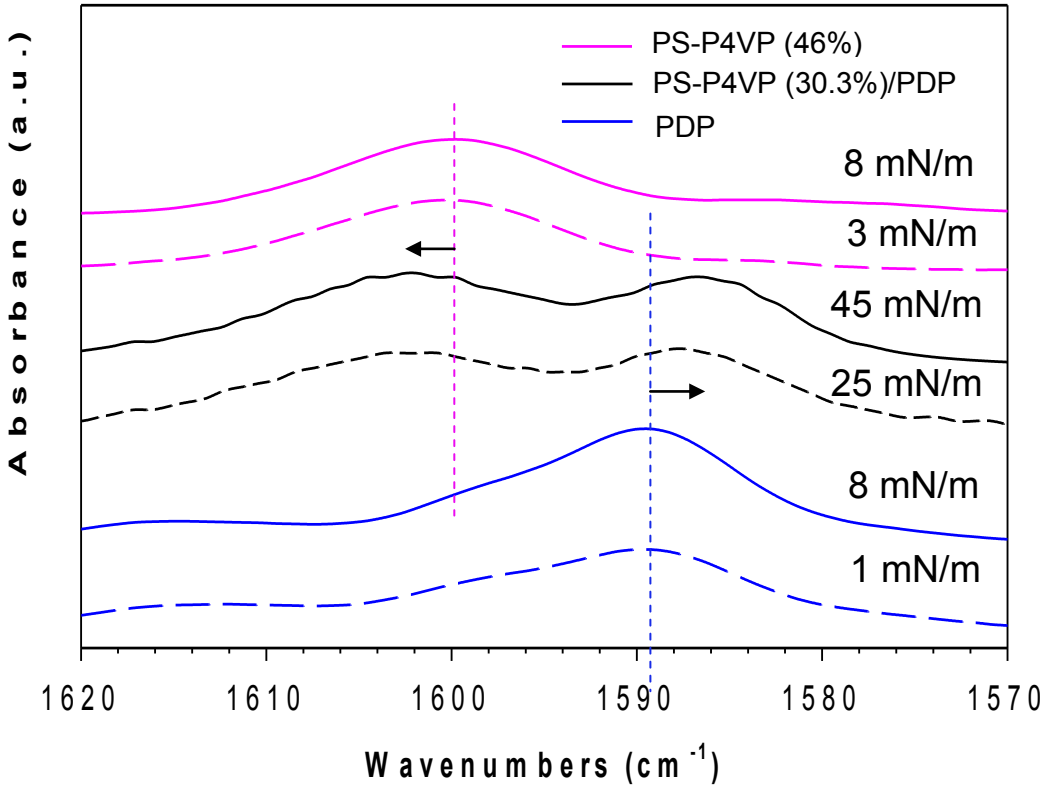

Figure 3-6. IR spectra in p-polarization for LB films of PDP, PS-P4VP(46%) and PS-P4VP(30.3%)/PDP transferred on silicon substrates at the surface pressures (π) indicated.

The P4VP band is located at 1598 cm^{-1} for pure P4VP (see Figure S4) and it is known to shift to higher frequency when hydrogen-bonded with PDP.[94] The amplitude of this shift has also been shown to be proportional to the strength of the supramolecular bond when other molecules are complexed.[48] This bands shifts to 1600 cm^{-1} for the LB films of the pure block copolymer, which is most likely due to the interaction of the pyridine ring with water molecules and/or with hydroxides on the silicon crystal surface. There is no noticeable difference whether the film was transferred below or above the plateau.

In the presence of PDP in the LB films of PS-P4VP(30.3%)/PDP, the band further shifts to around 1602 cm^{-1}. Table 3-8 highlights the similarity of the band position for the « p » and « s » polarizations (averaged over 3 different samples) and for films transferred at surface pressures of 25 and 45 mN/m. This implies that the level and/or strength of the complexation of the pyridine ring is similar for pyridine rings oriented parallel and perpendicular to the substrate and that there are no significant changes when increasing the transfer pressure above the isotherm plateau.

Table 3-9. Band positions of the P4VP pyridine ring and PDP phenol group for the transfer surface pressures (π) and polarizations (p or s) indicated.

Substance	**Band position cm^{-1}**	**π = 25 mN/m**		**π = 45 mN/m**	
		p	**s**	**p**	**s**
P4VP	1600	1602.45 ± 0.02	1601.83 ± 0.05	1602.1 ± 0.1	1601.7 ± 0.2
PDP	1587	1587.48 ± 0.04	1587.28 ± 0.06	1586.79 ± 0.02	1586.68 ±0.02

Figure 3-6 also shows that the position and the shape of the aromatic PDP band differs significantly in the spectra for pure PDP monolayers and when it is complexed with the pyridine ring. The band is located at 1589 cm^{-1} for the pure PDP monolayers, below and above the plateau (6 mN/m), which is similar to the melted bulk spectrum. This can be contrasted with the significant ordering of the PDP alkyl chains observed in Figure 3-4 when increasing the surface pressure to above the plateau. This result can be rationalized by considering the similarity of the intermolecular interactions. In the bulk, the phenol group of each PDP is H-bonded to other phenol groups. When prepared as monolayers, interactions with water molecules and/or silicon oxide or hydroxide groups likely dominate; however, these also involve oxygen atoms, leading to little change in interaction strength. On the other hand, when H-bonded to P4VP, the phenol groups are complexed to the nitrogen of the pyridine ring, which leads to a significant red shift of the band. Table 3-9 shows that the shift is greater above the isotherm plateau (1586.7 cm^{-1}) than below (1587.4 cm^{-1}), but that the position is not affected by polarization and thus by the orientation of the probed phenol groups. Figure S4 shows that an even greater shift, to 1586 cm^{-1}, occurs in the bulk complex.

3.2.3. Model describing the molecular rearrangement

The model shown in Figure 3-7 helps to explain the molecular-level information obtained from the infrared results in the context of the order-order transition of the dot morphology observed by AFM for PS-P4VP(30.3%)/PDP. In this scheme, the PS aggregates (or dots) are presented by the orange blobs; the P4VP chains and pyridine rings are shown in green and the PDP molecules are drawn in blue, where both P4VP and PDP make up the 2D monolayer matrix. In order for PS to avoid the water subphase with which it has little affinity, a monolayer of P4VP/PDP is expected to lie also under the PS aggregates.[71] In what follows, the explanations will focus on the transferred film, as analyzed by IR and AFM, but it is generally assumed in the literature that what is observed in the transferred films is also what existed at the air/water interface.

From the $<P_2>$ quantification of the C-H elongation of the PS benzene rings, it is clear that the PS chains in the blobs are isotropic, as expected. The hydrophilic and hydrophobic parts of the PDP molecules were analyzed separately, leading to the conclusion that the phenol groups are distributed isotropically at all surface pressures, while the alkyl chains, which are disordered with several gauche conformers, show an overall out-of-plane orientation with respect to the substrate that is essentially the same in films transferred below and above the isotherm plateau. In order to reduce the interfacial tension with air and taking into account the higher affinity of the phenol groups for the water subphase, the alkyl chains must tend to be oriented towards the air interface rather than towards the substrate surface (although $<P_2>$ values do not allow discriminating between these two possibilities). In the same vein, the pyridine rings show a global out-of-plane orientation with respect to the substrate for films transferred below the plateau pressure but are essentially isotropic above the transition. This initially surprising observation is rationalized in what follows.

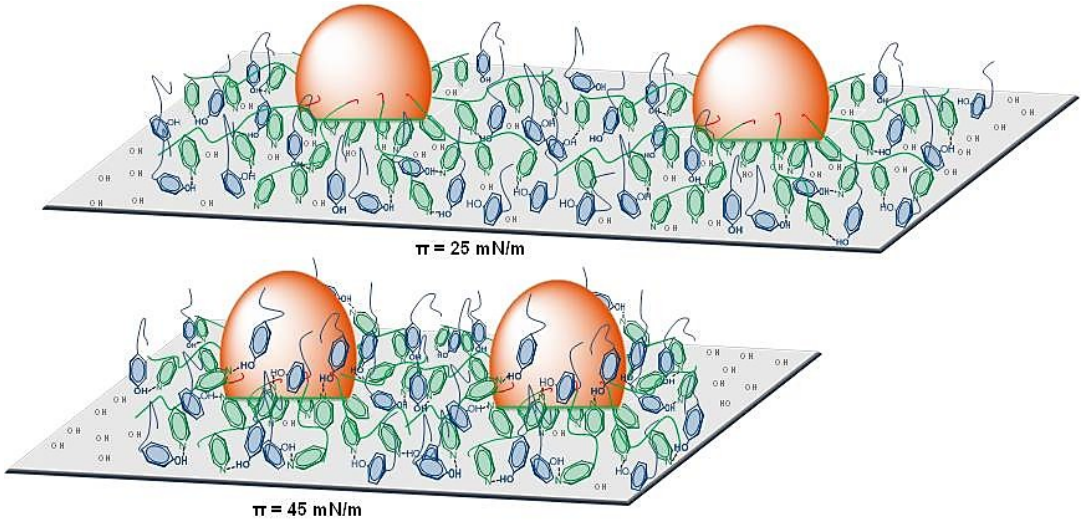

Figure 3-7. Model describing the molecular organization of the PS-P4VP(30.3%)/PDP system below and above the plateau pressure in the Langmuir isotherm. The dots, represented in orange, are composed of PS. The P4VP chains and PDP molecules are represented in green and blue, respectively. For samples transferred onto silicon substrates at a surface pressure of 25 mN/m, the pyridine rings and alkyl chains show a preferential orientation perpendicular to the surface. The pyridine rings and the phenol group of the PDP molecules are complexed either with the OH groups of the activated silicon substrate or with each other. For samples transferred at a surface pressure of 45 mN/m, only the alkyl chains preserve their parallel orientation with respect to the substrate normal. P4VP and PDP are mainly complexed together and the monolayer is partially collapsed, inducing an increase in the matrix thickness and increasing VP-OH hydrogen bonding.

The spectroscopic results showed a high level of hydrogen bonding both below and above the plateau pressure for both P4VP and PDP. From the pyridine point of view, the hydrogen-bond strength (indicated by the position of the 1600 cm^{-1} band in Figure 3-6) does not change with increasing surface pressure but, from

the PDP phenol point of view, the hydrogen-bond strength increases with increasing surface pressure. This can be understood by considering that, while the pyridine rings and the PDP molecules can interact with each other, they can also interact with the OH groups of the water surface (before transfer) and with the (plasma activated) silicon substrate and transferred water molecules after LB deposition. The pyridine band position is not strongly affected since OH groups are involved in all cases and give similar H-bonding strengths. On the other hand, the PDP phenol band is much more affected because of the significant differences in H-bonding strength with OH groups and with the nitrogen of the pyridine units (lower for OH···OH, higher for OH···pyridine). From a thermodynamic point of view, the pKa of the PDP molecules (close to 9) is lower than that of water, such that complexation of PDP to P4VP should be less favoured than to water. One must, however, consider the close proximity of P4VP and the PDP molecules in conditions where OH groups are "out-of-reach", which will favour VP-phenol H-bonding.

Below the plateau pressure, where the pyridine rings show out-of-plane orientation, it is reasonable to think that the nitrogen group of the pyridine rings is oriented towards the surface, thus favouring interactions with OH from water rather than with PDP. It can be assumed that the phenol groups also interact with the surface OH groups, and may be oriented; however, orientation in this case cannot be determined because of the rotational flexibility of the phenol OH group with respect to the aromatic ring.

When increasing the surface pressure to above the isotherm plateau, the matrix chains are compressed, inducing a significant reduction in the dot-to-dot distance. This causes a reorientation of the pyridine rings, which lose their preferential orientation along the substrate normal axis when the plateau pressure is reached. This can be explained by a kind of collapse of the monolayer between the PS dots from a thinner to a thicker layer of P4VP and PDP in which there is no preferred orientation. This decreases the possibility of hydrogen bonding with the substrate OH groups and favours P4VP-PDP hydrogen bonding, thus explaining

both the loss of pyridine orientation and the increased hydrogen-bonding strength observed for PDP above the plateau pressure.

It is reasonable to postulate that the pyridine group might undergo a change in orientation at the isotherm for pure PS-P4VP. However, this could not be verified by ATR-IR because of the low transfer ratio (0.2-0.5) of this system above the isotherm plateau.

3.2.4. Conclusions

To conclude, the molecular reorganization that accompanies the 2D order-order transition is related to a partial collapse of the P4VP monolayer and not to any reorientation of the PDP alkyl chains from prone to more vertical in the present system. This partial collapse implies loss of contact with the surface for a fraction of the pyridine groups, allowing increased H-bonding with PDP. The resulting matrix is essentially disordered, although, the alkyl chains are probably still located preferentially at the interface with air, since their molecular orientation is maintained. Presumably, the pure PS-P4VP block copolymer, which also shows a transition from hexagonal to square order for the dots, similarly experiences partial P4VP monolayer collapse above the much lower plateau pressure; however, the difference in thickness is too small to be detected by AFM. It must be emphasized that all of the measurements were done on transferred films, and in situ measurements at the air/water interface would be desirable to confirm that the observations for the transferred films reflect what occurred on the water surface. It should be mentioned again that Shin *et al.* reported an increase in trans conformation for alkyl side chains with increase in surface pressure using in situ IR.[76] This might be due to the compositional differences of their system relative to ours (covalently attached alkyl chains, ionic interactions due to quaternization, different alkyl chain length), but it might also be related to what occurs on the water surface and possible perturbation in ordering of the matrix during transfer to the solid substrate.

Appendix

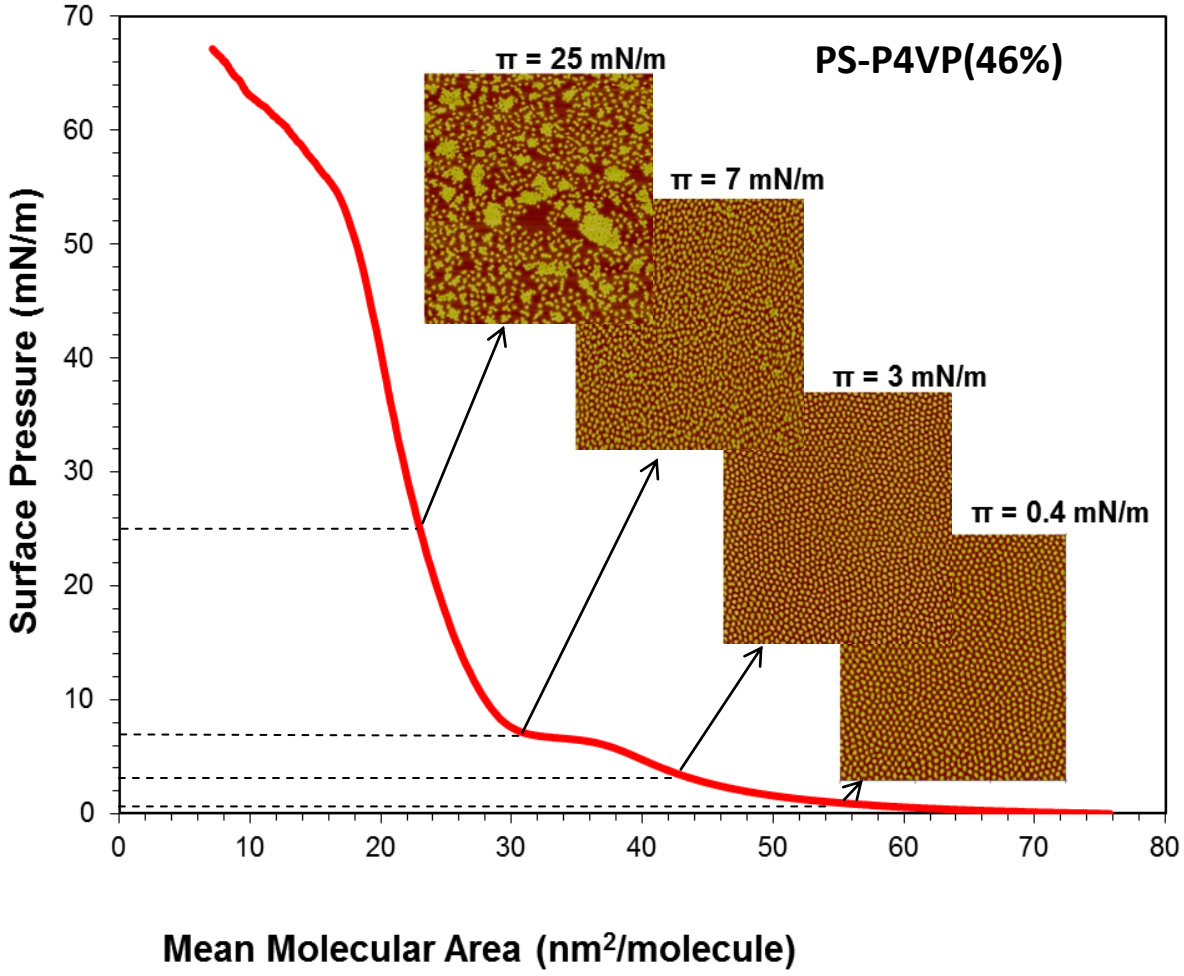

Figure S1. Langmuir compression isotherm of PS-P4VP(46%) at the air/water interface spreaded from the solution with concentration of 1.8 mg/mL. AFM height images (3x3 μm^2) of Langmuir-Blodgett monolayer films transferred on mica at the surface pressures (π) indicated.

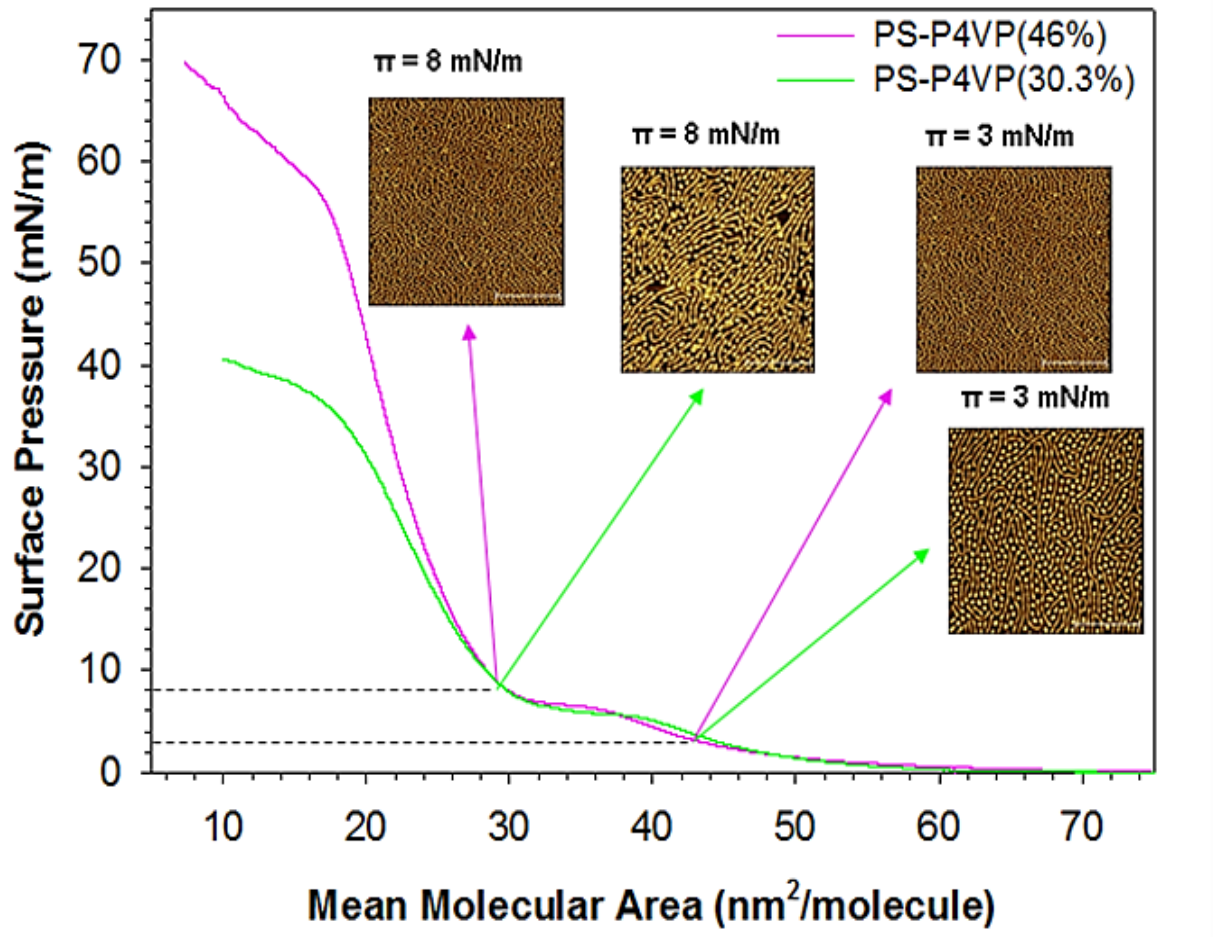

Figure S2. Langmuir compression isotherm of PS-P4VP(30.3%) (green curve) and PS-P4VP(46%) (purple curve) at the air/water interface. AFM height images (3x3 μm^2) of Langmuir-Blodgett monolayer films transferred on mica at the surface pressures (π) indicated. Solution concentration is 1.8 mg/mL.

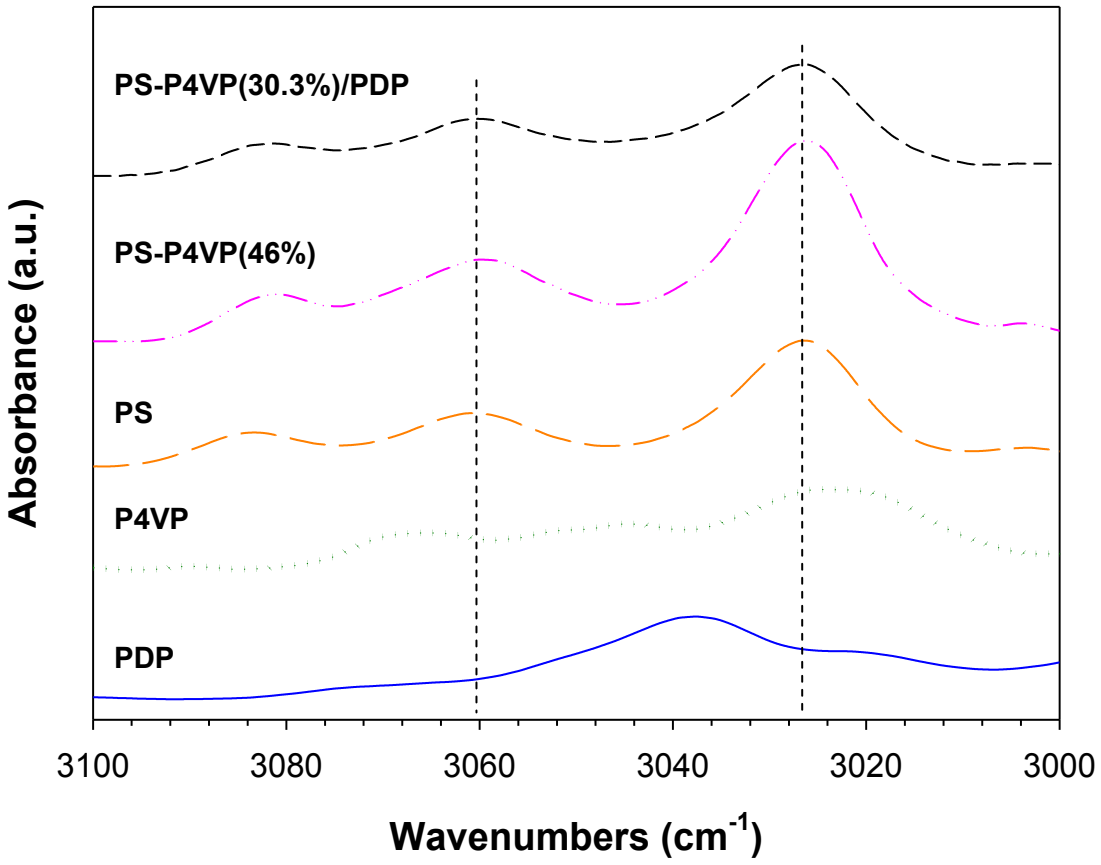

Figure S3. IR spectra of Langmuir-Blodgett PS-P4VP(30.5%)/PDP films transferred at a surface pressure of 45 mN/m in comparison to bulk spectra of pure melted PDP, P4VP, PS and the uncomplexed PS-P4VP(46%) copolymer.

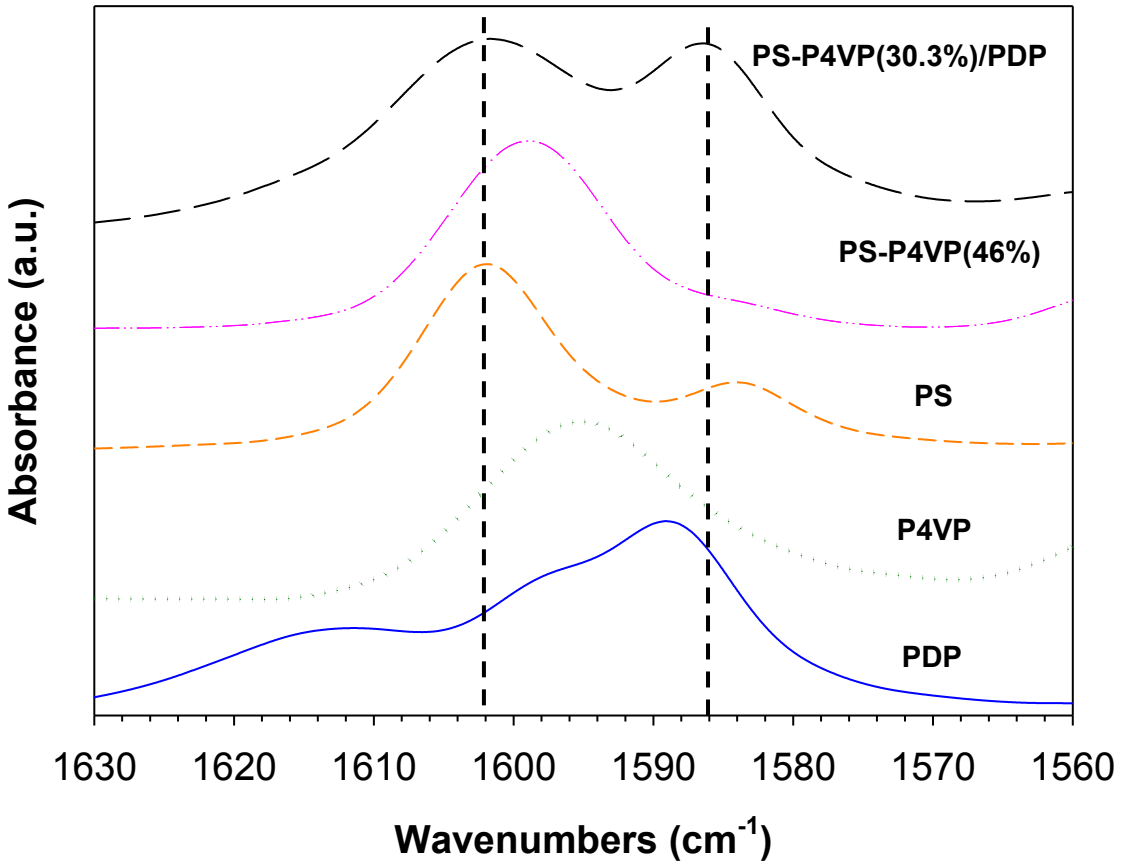

Figure S4. IR spectra of Langmuir-Blodgett PS-P4VP(30.3%)/PDP films transferred at a surface pressure of 45 mN/m in comparison to bulk spectra of pure melted PDP, P4VP, PS and the uncomplexed PS-P4VP(30.3%) copolymer.

CHAPTER 4

CONCLUSIONS AND FUTURE WORK

The current project was divided into two parts. The first objective (section 3.1) was to compare PS-P4VP alone with PS-P4VP complexed with naphthol and naphthoic acid, using the Langmuir-Blodgett technique (in contrast to the dip-coating technique that was used by S. Roland in work on the same systems) and to study the effect of spreading solution concentration on these systems. Langmuir isotherms and AFM images were obtained for five different solution concentrations (5, 2, 1, 0.5, 0.1 mg/mL). We showed that the presence or not of a plateau in the isotherm depends on the solution concentration in the case of the NOH- and NCOOH-containing systems (presence for low concentrations and absence for high concentrations). For the pure block copolymer, evidence of a plateau remains evident at the high concentrations, but in the form of a short diagonally oriented plateau. The plateau is located at low surface pressures (about 6 mN/m) for all three systems.

Previous work in the literature had established that amphiphilic block copolymers forming dots at the air/water interface typically show this plateau in Langmuir isotherms.[71,75] This is associated with a first-order phase transition, which was shown recently by Perepichka et al. to be an order-order transition of the dots from hexagonal order at low surface pressures to square order at high surface pressures.[74] In accordance with this, AFM images of LB films obtained below and above the plateau pressure in the present systems showed the hexagonal-like/square-like transition for the lower concentrations for the NOH- and NCOOH-containing solutions and the pure PS-P4VP system (regardless of the solution) concentration at the plateau. The high concentration small molecule-containing solutions developed an unclear (sponge-like for PS-P4VP/NOH and worm-like for PS-P4VP/NCOOH) morphology above the plateau pressure. This was postulated to be related to some compatibility of the small molecules, especially NOH, with the PS phase, which may allow greater fusion of the dots under higher pressure conditions. Pure PS-P4VP also shows significant clustering of the dots above the plateau at higher solution concentrations, but the square-like morphology is still perceptible, thus accounting for the still visible although short plateau in the Langmuir isotherm.

The second objective (section 3.2) was devoted to a deeper understanding of molecular changes that accompany the order-order achieving transition occuring at the isotherm plateau. This was done by applying infrared spectroscopic analysis to the Langmuir-Blodgett films of the PS-P4VP/PDP system deposited at low and high surface pressures. Previously, spectroscopic analysis at the air/water interface found that the trans conformation of alkyl side chains, in an alkylated PS-P4VP system, increased with surface pressure.[76,95] In our group, based on this reference and on AFM data showing that there are both low and higher regions of the P4VP/PDP matrix in LB films transferred very close to the plateau pressure, it was postulated that the alkyl chains of the PDP molecules reorient from prone to vertical position to account for the two matrix levels.[74]

By using polarized ATR-IR, we determined the orientation of different molecular moieties in the PS-P4VP/PDP system. We also deduced the effect of surface pressure on hydrogen bonding by examining relevant band shifts. Our IR analysis showed that no reorientation of the PDP alkyl chains takes place (the observed orientation is the same above and below the plateau pressure). On the other hand, the pyridine rings have out-of-plane orientation at low surface pressure and become isotropic above the plateau pressure. Furthermore, increased hydrogen-bonding between PDP and P4VP was deduced from the band shifts involving the phenol group of PDP.

This led to the proposal of a new model to explain what occurs at the molecular level during the order-order transition. Essentially, the data can be rationalized by postulating a partial collapse of the P4VP monolayer at the transition, which occurs due to the lateral pressure on the surface film. This partial collapse is visualized as the P4VP, which, along with PDP, is in the form of a monolayer hugging the water surface at low pressure (thus also rationalizing the observed orientation of the pyridine), transforming into a thin multilayer at the plateau. Such a collapse involves a loss of contact of a fraction of the pyridine groups with the substrate surface and consequent loss of pyridine orientation along with greater H-bonding with PDP molecules (and less with the OH groups of the water or silicon surface).

To follow up this work, it is desirable to validate the mechanism directly at the air/water interface by using the technique of polarized infrared reflection–absorption spectroscopy (IRRAS). (This apparatus is currently in the process of being installed with an LB bath in our laboratories.) For example, it is possible that the lack of reorientation of the PDP alkyl chains is a result of disorder occuring during the monolayer transfer to the solid substrate. If lack of order is confirmed at the air/water interface, then it will be of interest to examine the system as used in ref. 77 to determine if reorientation (or greater trans character) occurs with covalently attached alkyl chains. It is also desirable, in the NOH- and NCOOH-containing systems, to verify by IR if the small molecule content is the same below and above the plateau pressure to address the question of possible solubilization in the water phase at higher pressure (either *in situ* or after LB transfer or both, since there may also be some evaporation of the small molecule after LB transfer).

In this connection, it is of interest to mention preliminary work with another small molecule, octylbenzoic acid (OBA), mixed with PS-P4VP. This system (PS-P4VP(30%)/OBA, using a chloroform solution with a concentration of 1.8 mg/mL) showed an unusual Langmuir isotherm that has convex character in the surface pressure region of 10-20 mN/m as well as a short plateau at about 36 mN/m, as shown in Figure 4-1. The corresponding AFM images of LS films deposited at different surface pressures, and presented in Figure 4-1, show hexagonal dot order up to at least 15 mN/m, but square order appears to have already developed by 30 mN/m (below the short plateau), suggesting that the convex region may be related to that change. But it is also postulated that some OBA may dissolve into the water subphase with increase in surface pressure due to the short alkyl chain,[96] which might be another reason for the form of the isotherm below the short plateau. This system merits more detailed investigation, including by IR analysis as above and in situ at the air/water interface, along with determination of any alkyl chain orientation and change in hydrogen-bonding characteristics (the strongly absorbing carbonyl group, in particular, which is sensitive to hydrogen-bonding, should be relatively easily detectable).

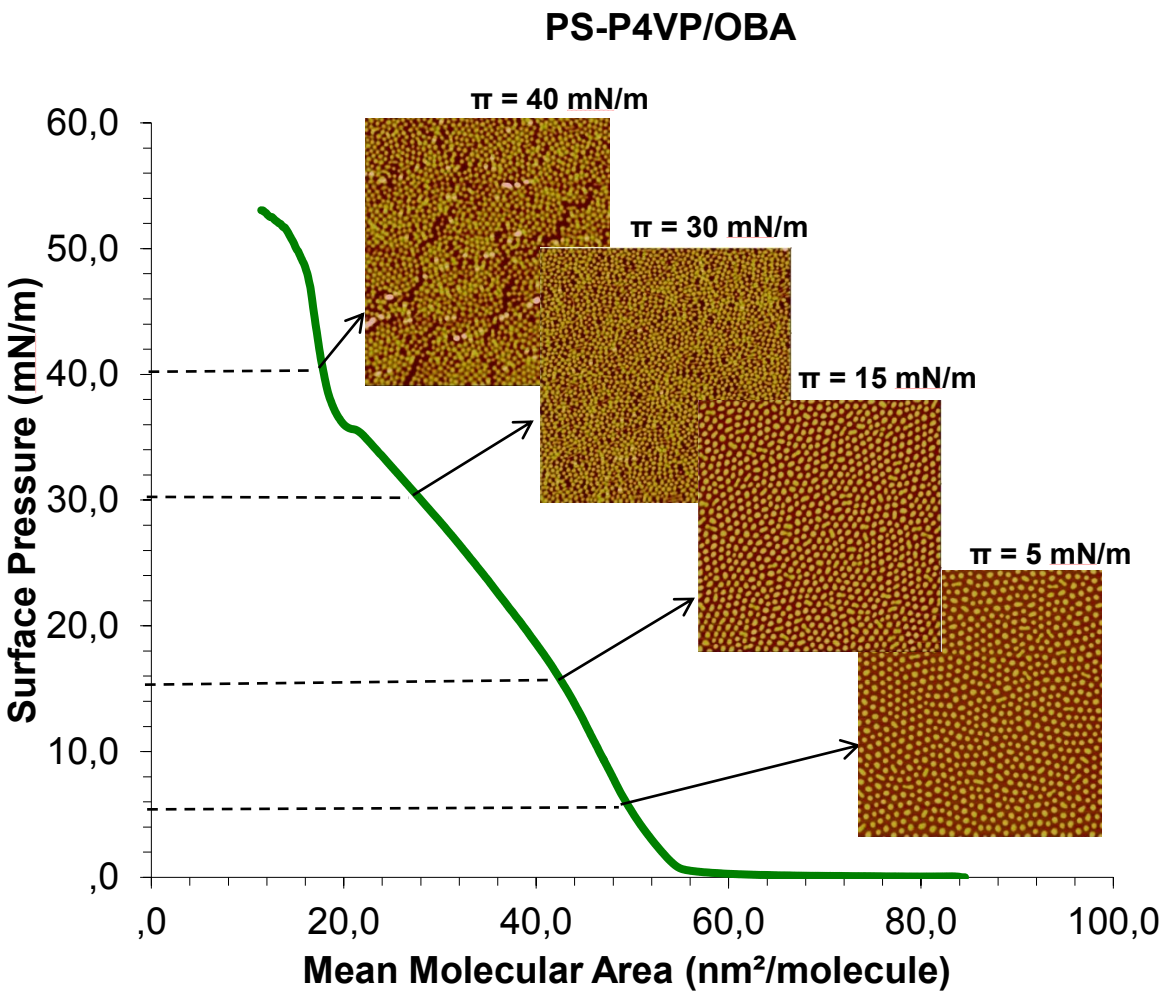

Figure4-1. Langmuir compression isotherm of PS-P4VP(30%)/OBA system spread from $CHCl_3$ solution (1.8 mg/mL) at 21±0.5ºC. AFM height images (3x3 μm^2) of Langmuir-Schaefer monolayer films transferred on mica at the surface pressures (π) indicated.

Finally, returning to the system with PDP, it is of interest to study this system in the form of dip-coated films. This idea is based on the work of Roland *et al.* who studied the morphology of dip-coated films of PS-P4VP/NOH and PS-P4VP/NCOOH systems deposited at different dip-coating rates, which, as

mentioned in section 1.2, leads to films with different morphologies.[39] So far, all such studies have involved small molecules that do not crystallize when hydrogen-bonded to P4VP. However, the PDP alkyl chains are long enough to crystallize (and show liquid crystalline character above the melting point) while also being hydrogen-bonded to P4VP.[94] How this might reveal itself in dip-coated films and how it might influence the morphologies in such films will be interesting to investigate.

Lastly, it should be added that patterned films, whether obtained by LB/LS techniques or by dip-coating (or otherwise), have potential usefulness as templates for gold array fabrication (in the case of hexagonal dot morphology) or gold nanowire fabrication (in the case of nanostrand structure). Such templates are expected to show greater optical properties and can be applied widely in nanotechnologies. Thus, any method and underlying understanding that allows greater control and finer manipulation of these patterns is of great value.

References

1. Schmid, G., *Nanotechnology: Principles and Fundamentals*. Wiley-VCH: Oakland, USA, **2008**.

2. Nalwa, H. S., *Encyclopedia of nanoscience and nanotechnology. v. 1-10*. American Scientific Publishers: Stevenson Ranch, USA, **2004**.

3. Whitesides, G. M.; Grzybowski, B., Self-Assembly at All Scales. *Science* **2002,** *295*, 2418-2421.

4. Calladine, C. R.; Drew, H.; Luisi, B.; Travers, A., *Understanding DNA: The Molecule and How it Works*. Elsevier Science: Waltham, USA, **2004**.

5. Berg, J. M.; Tymoczko, J. L.; Stryer, L., *Biochemistry,* Fifth Edition. W.H. Freeman: London, UK, **2002**.

6. Schlick, T. L.; Ding, Z. B.; Kovacs, E. W.; Francis, M. B., Dual-Surface Modification of the Tobacco Mosaic Virus. *J. Am. Chem. Soc.* **2005,** *127*, 3718-3723.

7. Howland, J., Biochemistry: By D. Voet and J. G. Voet. John Wiley and Sons: New York, *Biochem. Educ.* **1990,** *18*, 1223.

8. Hirth, L.; Lebeurier, G.; Nicolaieff, A.; Richards, K., The Self-Assembly of Tobacco Mosaic Virus: Influence of the Viral RNA and DNA Protein Components Upon the Assembly Process. *Biophys. J.* **1980,** *32*, 460-462.

9. Philp, D.; Stoddart, J. F., Self-Assembly in Natural and Unnatural Systems. *Angew. Chem. Int. Ed. (English)* **1996,** *35*, 1154-1196.

10. Hamley, I. W., Nanostructure Fabrication Using Block Copolymers. *Nanotechnology* **2003,** *14*, R39-R54.

11. Lazzari, M.; Lopez-Quintela, M. A., Block Copolymers as a Tool for Nanomaterial Fabrication. *Adv. Mater.* **2003,** *15*, 1583-1594.

12. Fasolka, M. J.; Mayes, A. M., Block Copolymer Thin Films: Physics and Applications. *Annu. Rev. Mater. Res.* **2001,** *31*, 323-355.

13. Kim, J. K.; Lee, J. I.; Lee, D. H., Self-Assembled Block Copolymers: Bulk to Thin Film. *Macromol. Res.* **2008,** *16*, 267-292.

14. Mai, Y. Y.; Eisenberg, A., Self-Assembly of Block Copolymers. *Chem. Soc. Rev.* **2012,** *41*, 5969-5985.

15. Bates, F. S.; Fredrickson, G. H., Block Copolymers - Designer Soft Materials. *Phys. Today* **1999,** *52*, 32-38.

16. Bates, F. S., Polymer-Polymer Phase Behavior. *Science* **1991,** *251*, 898-905.

17. Fahmi, A. W.; Braun, H. G.; Stamm, M., Fabrication of Metallized Nanowires from Self-Assembled Diblock Copolymer Templates. *Adv. Mater.* **2003,** *15*, 1201-1204.

18. Alberda van Ekenstein, G.; Polushkin, E.; Nijland, H.; Ikkala, O.; ten Brinke, G., Shear Alignment at Two Length Scales: Comb-Shaped Supramolecules Self-Organized as Cylinders-Within-Lamellar Hierarchy. *Macromolecules* **2003,** *36*, 3684-3688.

19. de Moel, K.; Alberda van Ekenstein, G. O. R.; Nijland, H.; Polushkin, E.; ten Brinke, G.; Maeki-Ontto, R.; Ikkala, O., Polymeric Nanofibers Prepared from Self-Organized Supramolecules. *Chem. Mater.* **2001,** *13*, 4580-4583.

20. Mäki-Ontto, R.; de Moel, K.; de Odorico, W.; Ruokolainen, J.; Stamm, M.; ten Brinke, G.; Ikkala, O., "Hairy Tubes": Mesoporous Materials Containing Hollow Self-Organized Cylinders with Polymer Brushes at the Walls. *Adv. Mater.* **2001,** *13*, 117-121.

21. Park, M.; Harrison, C.; Chaikin, P. M.; Register, R. A.; Adamson, D. H., Block Copolymer Lithography: Periodic Arrays of Similar to 10(11) Holes in 1 Square Centimeter. *Science* **1997,** *276*, 1401-1404.

22. Park, M.; Chaikin, P. M.; Register, R. A.; Adamson, D. H., Large Area Dense Nanoscale Patterning of Arbitrary Surfaces. *Appl. Phys. Lett.* **2001,** *79*, 257-259.

23. Misner, M. J.; Skaff, H.; Emrick, T.; Russell, T. P., Directed Deposition of Nanoparticles Using Diblock Copolymer Templates. *Adv. Mater.* **2003,** *15*, 221-224.

24. Nandan, B.; Gowd, E. B.; Bigall, N. C.; Eychmuller, A.; Formanek, P.; Simon, P.; Stamm, M., Arrays of Inorganic Nanodots and Nanowires Using Nanotemplates Based on Switchable Block Copolymer Supramolecular Assemblies. *Adv. Funct. Mater.* **2009,** *19*, 2805-2811.

25. Lee, D. H.; Shin, D. O.; Lee, W. J.; Kim, S. O., Hierarchically Organized Carbon Nanotube Arrays From Self-Assembled Block Copolymer Nanotemplates. *Adv. Mater.* **2008,** *20*, 2480-2485.

26. Yang, S. Y.; Ryu, I.; Kim, H. Y.; Kim, J. K.; Jang, S. K.; Russell, T. P., Nanoporous Membranes With Ultrahigh Selectivity and Flux For the Filtration of Viruses. *Adv. Mater.* **2006,** *18*, 709-712.

27. Yang, S. Y.; Yang, J. A.; Kim, E. S.; Jeon, G.; Oh, E. J.; Choi, K. Y.; Hahn, S. K.; Kim, J. K., Single-File Diffusion of Protein Drugs Through Cylindrical Nanochannels. *ACS Nano* **2010,** *4*, 3817-3822.

28. Alexandridis, P.; Lindman, B., *Amphiphilic Block Copolymers: Self-Assembly and Applications*. Elsevier Science: Amsterdam, Netherlands, **2000**.

29. Lodge, T. P.; Pudil, B.; Hanley, K. J., The Full Phase Behavior For Block Copolymers in Solvents of Varying Selectivity. *Macromolecules* **2002,** *35*, 4707-4717.

30. Hanley, K. J.; Lodge, T. P.; Huang, C. I., Phase Behavior of a Block Copolymer in Solvents of Varying Selectivity. *Macromolecules* **2000,** *33*, 5918-5931.

31. Choi S. Block Copolymer Self-Assembly in Solution: Structure and Dynamics, Ph.D Thesis, Department of Chemical Engineering and Materials Science, University of Minnesota, **2010**.

32. Kosonen, H.; Ruokolainen, J.; Knaapila, M.; Torkkeli, M.; Serimaa, R.; Bras, W.; Monkman, A. P.; ten Brinke, G.; Ikkala, O., Self-Organized Supermolecules Based on Conducting Polyaniline and Hydrogen Bonded Amphiphiles. *Synth. Met.* **2001,** *121*, 1277-1278.

33. Chao, C. Y.; Li, X. F.; Ober, C. K.; Osuji, C.; Thomas, E. L., Orientational Switching of Mesogens and Microdomains in Hydrogen-Bonded Side-Chain Liquid-Crystalline Block Copolymers Using AC Electric Fields. *Adv. Funct. Mater.* **2004,** *14*, 364-370.

34. Huang, C. M.; Wei, K. H.; Jeng, U. S.; Liang, K. S., Structural Evolution of Poly(styrene-b-4-vinylpyridine) Diblock Copolymer/Gold Nanoparticle Mixtures From Solution to Solid State. *Macromolecules* **2007,** *40*, 5067-5074.

35. van Zoelen, W.; Asumaa, T.; Ruokolainen, J.; Ikkala, O.; ten Brinke, G., Phase Behavior of Solvent Vapor Annealed Thin Films of PS-b-P4VP(PDP) Supramolecules. *Macromolecules* **2008,** *41*, 3199-3208.

36. Ruokolainen, J.; Saariaho, M.; Ikkala, O.; ten Brinke, G.; Thomas, E. L.; Torkkeli, M.; Serimaa, R., Supramolecular Routes to Hierarchical Structures: Comb-Coil Diblock Copolymers Organized With Two Length Scales. *Macromolecules* **1999,** *32*, 1152-1158.

37. Bharatiya, B.; Schumers, J. M.; Poggi, E.; Gohy, J. F., Supramolecular Assemblies from Poly(styrene)-block-poly(4-vinylpyridine) Diblock Copolymers Mixed with 6-Hydroxy-2-naphthoic Acid. *Polymers.* **2013,** *5*, 679-695.

38. Tokarev, I.; Krenek, R.; Burkov, Y.; Schmeisser, D.; Sidorenko, A.; Minko, S.; Stamm, M., Microphase Separation in Thin Films of Poly(styrene-block-4-vinylpyridine) Copolymer-2-(4'-hydroxybenzeneazo)benzoic Acid Assembly. *Macromolecules* **2005,** *38*, 507-516.

39. Roland, S.; Gaspard, D.; Prud'homme, R. E.; Bazuin, C. G., Morphology Evolution in Slowly Dip-Coated Supramolecular PS-b-P4VP Thin Films. *Macromolecules* **2012,** *45*, 5463-5476.

40. Perepichka, I. I.; Lu, Q.; Badia, A.; Bazuin, C. G., Understanding and Controlling Morphology Formation in Langmuir-Blodgett Block Copolymer Films Using PS-P4VP and PS-P4VP/PDP. *Langmuir* **2013,** *29*, 4502-4519.

41. Valkama, S.; Ruotsalainen, T.; Nykanen, A.; Laiho, A.; Kosonen, H.; ten Brinke, G.; Ikkala, O.; Ruokolainen, J., Self-Assembled Structures in Diblock Copolymers With Hydrogen-Bonded Amphiphilic Plasticizing Compounds. *Macromolecules* **2006,** *39*, 9327-9336.

42. Ruotsalainen, T.; Turku, J.; Hiekkataipale, P.; Vainio, U.; Serimaa, R.; ten Brinke, G.; Harlin, A.; Ruokolainen, J.; Ikkala, O., Tailoring of the Hierarchical Structure Within Electrospun Fibers Due to Supramolecular Comb-Coil Block Copolymers: Polystyrene-Block-Poly(4-vinyl pyridine) Plasticized by Hydrogen Bonded Pentadecylphenol. *Soft Matter.* **2007,** *3*, 978-985.

43. Tung, S.-H.; Kalarickal, N. C.; Mays, J. W.; Xu, T., Hierarchical Assemblies of Block-Copolymer-Based Supramolecules in Thin Films. *Macromolecules* **2008,** *41*, 6453-6462.

44. Huang, W.-H.; Chen, P.-Y.; Tung, S.-H., Effects of Annealing Solvents on the Morphology of Block Copolymer-Based Supramolecular Thin Films. *Macromolecules* **2012,** *45*, 1562-1569.

45. van Zoelen, W.; Asumaa, T.; Ruokolainen, J.; Ikkala, O.; ten Brinke, G., Phase Behavior of Solvent Vapor Annealed Thin Films of PS-b-P4VP(PDP) Supramolecules. *Macromolecules* **2008,** *41*, 3199-3208.

46. van Zoelen, W.; Bondzic, S.; Landaluce, T. F.; Brondijk, J.; Loos, K.; Schouten, A.-J.; Rudolf, P.; ten Brinke, G., Nanostructured Polystyrene-Block-Poly(4-vinyl pyridine)(pentadecylphenol) Thin Films as Templates For Polypyrrole Synthesis. *Polymer* **2009,** *50*, 3617-3625.

47. Nandan, B.; Vyas, M. K.; Bohme, M.; Stamm, M., Composition-Dependent Morphological Transitions and Pathways in Switching of Fine Structure in Thin Films of Block Copolymer Supramolecular Assemblies. *Macromolecules* **2010,** *43*, 2463-2473.

48. Roland, S.; Pellerin, C.; Bazuin, C. G.; Prud'homme, R. E., Evolution of Small Molecule Content and Morphology with Dip-Coating Rate in Supramolecular PS-P4VP Thin Films. *Macromolecules* **2012,** *45*, 7964-7972.

49. Roland, S.; Prud'homme, R. E.; Bazuin, C. G., Morphology, Thickness, and Composition Evolution in Supramolecular Block Copolymer Films over a Wide Range of Dip-Coating Rates. *ACS Macro Letters* **2012,** *1*, 973-976.

50. Pockels, A., Surface Tension. *Nature* **1891,** *43*, 437-439.

51. Langmuir, I., Constitution and Fundamental Properties of Solids and Liquids. II. Liquids. *J. Am. Chem. Soc.* **1917,** *39*, 1848-1906.

52. Greene, J. E., Organic Thin Films: From Monolayers on Liquids to Multilayers on Solids. *Phys. Today* **2014,** *67*, 43-48.

53. Roberts, G., *Langmuir-Blodgett Films*. Springer New York, US: **1990**.

54. Gaines, G. L., *Insoluble Monolayers at Liquid-gas Interfaces*. Interscience Publisher: New York, US, 1966.

55. Girard-Egrot, A.; Blum, L., Langmuir-Blodgett Technique for Synthesis of Biomimetic Lipid Membranes. In *Nanobiotechnology of Biomimetic Membranes*, Martin, D., Ed. Springer: New York, US, **2007**; Vol. 1, pp 23-74.

56. Hussain, S. A., Langmuir-Blodgett Films a Unique Tool For Molecular Electronics. *arXiv.org, e-Print Arch., Phys.* **2009**, 1-9, arXiv:0908.1814v1 [physics.gen-ph].

57. Oliveira, O. N., Jr., Langmuir-Blodgett Films - Properties and Possible Applications. *Braz. J. Phys.* **1992,** *22*, 60-69.

58. Hann, R. A., Molecular Structure and Monolayer Properties. In *Langmuir-Blodgett Films*, Roberts, G., Ed. Springer: New York, US, **1990**; pp 17-92.

59. Tanaka, K.; Okahata, Y., Evaluation of a Horizontal Lifting Method of LB Films by Using a Quartz-Crystal Microbalance. *Kagaku Kogyo* **1992,** *43*, 230-235.

60. Langmuir, I.; Schaefer, V. J., Activities of Urease and Pepsin Monolayers. *J. Am. Chem. Soc.* **1938,** *60*, 1351-1360.

61. Stuart, B. H., *Infrared Spectroscopy: Fundamentals and Applications*. Wiley: New York, US, **2004**.

62. Smith, B. C., *Fundamentals of Fourier Transform Infrared Spectroscopy,* Second Edition. CRC Press: Boca Raton, US, **2011**.

63. Chalmers, J. M.; Meier, R. J., *Molecular Characterization and Analysis of Polymers*. Elsevier Science: Amsterdam, Netherlands, **2008**.

64. Buffeteau, T.; Le Calvez, E.; Desbat, B.; Pelletier, I.; Pezolet, M., Quantitative Orientation of α-Helical Polypeptides by Attenuated Total Reflection Infrared Spectroscopy. *J. Phys. Chem. B* **2001,** *105*, 1464-1471.

65. Fringeli, U. P.; Günthard, H. H., Infrared Membrane Spectroscopy. In *Membrane Spectroscopy*, Grell, E., Ed. Springer: Berlin Heidelberg, **1981**; Vol. 31, pp 270-332.

66. Citra, M. J.; Axelsen, P. H., Determination of Molecular Order in Supported Lipid Membranes by Internal Reflection Fourier Transform Infrared Spectroscopy. *Biophys. J.* **1996,** *71*, 1796-1805.

67. Chalmers, J. M.; Griffiths, P. R., *Handbook of Vibrational Spectroscopy*. J. Wiley: Chichester, England, **2002**.

68. Harrick, N. J., *Internal Reflection Spectroscopy*. Interscience Publishers: New York, US, **1967**.

69. Zhu, J.; Eisenberg, A.; Lennox, R. B., Interfacial Behavior of Block Polyelectrolytes. 5. Effect of Varying Block Lengths on the Properties of Surface Micelles. *Macromolecules* **1992,** *25*, 6547-6555.

70. Li, S.; Clarke, C. J.; Lennox, R. B.; Eisenberg, A., Two-Dimensional Self Assembly of Polystyrene-b-Poly (butyl-methacrylate) Diblock Copolymers. *Colloids Surf., A* **1998,** *133*, 191-203.

71. Perepichka, I. I.; Lu, Q.; Badia, A.; Bazuin, C. G., Understanding and Controlling Morphology Formation in Langmuir–Blodgett Block Copolymer Films Using PS-P4VP and PS-P4VP/PDP. *Langmuir* **2013,** *29*, 4502-4519.

72. Lu, Q.; Bazuin, C. G., Solvent-Assisted Formation of Nanostrand Networks from Supramolecular Diblock Copolymer/Surfactant Complexes at the Air/Water Interface. *Nano Lett.* **2005,** *5*, 1309-1314.

73. Perepichka, I. I.; Badia, A.; Bazuin, C. G., Nanostrand Formation of Block Copolymers at the Air/Water Interface. *ACS Nano* **2010,** *4*, 6825-6835.

74. Perepichka, I. I.; Borozenko, K.; Badia, A.; Bazuin, C. G., Pressure-Induced Order Transition in Nanodot-Forming Diblock Copolymers at the Air/Water Interface. *J. Am. Chem. Soc.* **2011,** *133*, 19702-19705.

75. Zhu, J. Y.; Eisenberg, A.; Lennox, R. B., Interfacial Behavior of Block Polyelectrolytes .1. Evidence for Novel Surface Micelle Formation. *J. Am. Chem. Soc.* **1991,** *113*, 5583-5588.

76. Shin, K.; Rafailovich, M. H.; Sokolov, J.; Chang, D. M.; Cox, J. K.; Lennox, R. B.; Eisenberg, A.; Gibaud, A.; Huang, J.; Hsu, S. L.; Satija, S. K., Observation of Surface Ordering of Alkyl Side Chains in Polystyrene/Polyelectrolytes Diblock Copolymer Langmuir Films. *Langmuir* **2001,** *17*, 4955-4961.

77. Glagola, C. P.; Miceli, L. M.; Milchak, M. A.; Halle, E. H.; Logan, J. L., Polystyrene-Poly(ethylene oxide) Diblock Copolymer: The Effect of Polystyrene and Spreading Concentration at the Air/Water Interface. *Langmuir* **2012,** *28*, 5048-5058.

78. Langmuir, I.; Schaefer, V. J., Activities of Urease and Pepsin Monolayers. *J. Am. Chem. Soc.* **1938,** *60*, 1351-1360.

79. Zhu, J. Y.; Lennox, R. B.; Eisenberg, A., Polymorphism of (Quasi) 2-Dimensional Micelles. *J. Phys. Chem.***1992,** *96*, 4727- 4730.

80. Perepichka, I. I., Self-Assembly of PS-PVP Block Copolymers and Their Complexes at the Air/Water Interface. Ph.D. Thesis, Department of Chemistry, Université de Montréal, **2011**.

81. Li, S.; Clarke, C. J.; Eisenberg, A.; Lennox, R. B., Langmuir Films of Polystyrene-b-Poly(alkyl acrylate) Diblock Copolymers. *Thin Solid Films* **1999,** *354*, 136-141.

82. Kawaguchi, M.; Itoh, S.; Takahashi, A., Liquid-Expanded to Liquid-Condensed Phase Transition in Polyelectrolyte Monolayers on the Aqueous KBr Solution. 2. Temperature Dependence. *Macromolecules* **1987,** *20*, 1052-1060.

83. Kawaguchi, M.; Itoh, S.; Takahashi, A., Liquid-Expanded to Liquid-Condensed Phase Transition in Polyelectrolyte Monolayers on the Aqueous KBr Solution. 1. Salt Concentration Dependence. *Macromolecules* **1987,** *20*, 1056-1060.

84. Seo, Y.; Paeng, K.; Park, S., Molecular Weight Effect on the Behaviors of Polystyrene-block-poly(methyl methacrylate) Diblock Copolymers at Air/Water Interface. *Macromolecules* **2001,** *34*, 8735-8744.

85. Wang, X.; Ma, X.; Zang, D., Aggregation Behavior of Polystyrene-b-Poly(acrylic acid) at the Air-Water Interface. *Soft Matter.* **2013,** *9*, 443-453.

86. Cox, J. K.; Yu, K.; Eisenberg, A.; Bruce Lennox, R., Compression of Polystyrene-Poly(ethylene oxide) Surface Aggregates at the Air/Water Interface. *Phys. Chem. Chem. Phys.* **1999,** *1*, 4417-4421.

87. Allara, D. L.; Swalen, J. D., An Infrared Reflection Spectroscopy Study of Oriented Cadmium Arachidate Monolayer Films on Evaporated Silver. *J. Phys. Chem.* **1982,** *86*, 2700-2704.

88. Porter, M. D.; Bright, T. B.; Allara, D. L.; Chidsey, C. E. D., Spontaneously Organized Molecular Assemblies. 4. Structural Characterization of N-alkyl Thiol Monolayers on Gold by Optical Ellipsometry, Infrared Spectroscopy, and Electrochemistry. *J. Am. Chem. Soc.* **1987,** *109*, 3559-3568.

89. Jasse, B.; Koenig, J. L., Fourier Transform Infra-Red Study of Uniaxially-Oriented Isotactic Polystyrene. *Polymer* **1981,** *22*, 1040-1044.

90. Panov, V. P.; Kazarin, L. A.; Dubrovin, V. I.; Gusev, V. V.; Kirsh, Y. É., Infrared Spectra of Atactic Poly-4-Vinylpyridine. *J. Appl. Spectrosc.* **1974,** *21*, 1504-1510.

91. Lee, S. W.; Chae, B.; Hahm, S. G.; Lee, B.; Kim, S. B.; Ree, M., Rubbed Films of Isomeric Poly(4-vinylpyridine) and Poly(2-vinylpyridine): Surface Morphology, Molecular Orientation, and Liquid Crystal Alignability. *Polymer* **2005,** *46*, 4068-4076.

92. Richard-Lacroix, M.; Pellerin, C., Novel Method for Quantifying Molecular Orientation by Polarized Raman Spectroscopy: a Comparative Simulations Study. *Appl. Spectrosc.* **2013,** *67*, 409-419.

93. Richard-Lacroix, M.; Pellerin, C., Accurate New Method for Molecular Orientation Quantification Using Polarized Raman Spectroscopy. *Macromolecules* **2013,** *46*, 5561-5569.

94. Ruokolainen, J.; ten Brinke, G.; Ikkala, O.; Torkkeli, M.; Serimaa, R., Mesomorphic Structures in Flexible Polymer−Surfactant Systems Due to Hydrogen Bonding: Poly(4-vinylpyridine)−Pentadecylphenol. *Macromolecules* **1996,** *29*, 3409-3415.

95. Dicko, A.; Bourque, H.; Pézolet, M., Study by Infrared Spectroscopy of The Conformation of Dipalmitoylphosphatidylglycerol Monolayers at the Air–Water Interface and Transferred on Solid Substrates. *Chem. Phys. Lipids* **1998,** *96*, 125-139.

96. Friberg, S. E., *Interactions of Surfactants with Polymers and Proteins*, CRC Press: Boca Raton, US, **1993.**